NASA Technical Memorandum 78699

Comparison of Wing-Span Averaging Effects on Lift, Rolling Moment, and Bending Moment for Two Span Load Distributions and for Two Turbulence Representations

Jacob H. Lichtenstein

SEPTEMBER 1978

NASA

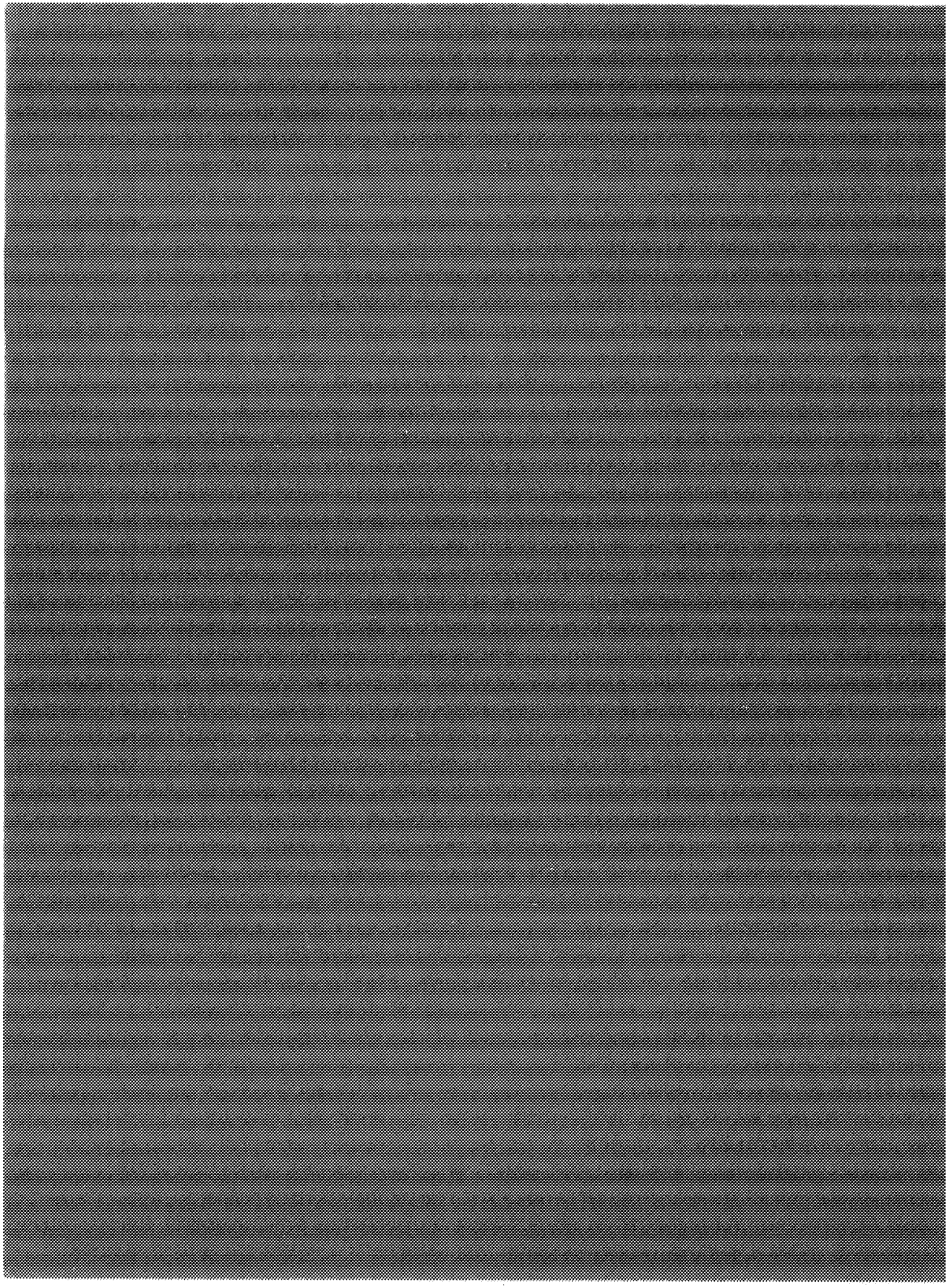

NASA Technical Memorandum 78699

Comparison of Wing-Span Averaging Effects on Lift, Rolling Moment, and Bending Moment for Two Span Load Distributions and for Two Turbulence Representations

Jacob H. Lichtenstein
Langley Research Center
Hampton, Virginia

National Aeronautics
and Space Administration

**Scientific and Technical
Information Office**

1978

SUMMARY

An analytical method of computing the averaging effect of wing-span size on the loading of a wing induced by random turbulence was adapted for use on a digital electronic computer. The turbulence input was assumed to have a Dryden power spectral density. The computations were made for lift, rolling moment, and bending moment for two span load distributions, rectangular and elliptic.

The results show that the wing-span averaging effect increased with both span size and turbulence frequency. The rectangular wing-span loading showed a slightly greater averaging effect than did the elliptic loading. In the frequency range most bothersome to airplane passengers, the wing-span averaging effect can reduce the normal lift load, and thus the acceleration, by about 7 percent for a typical medium-sized transport. The bending moment exhibited results similar to those for the lift but to a lesser degree. The rolling moment exhibited its greatest effect at low frequencies and small wing-span sizes. Some calculations were made to evaluate the effect of using a Von Karman turbulence representation. These results showed that using the Von Karman representation generally resulted in a span averaging effect about 3 percent larger.

INTRODUCTION

The gust loads on airplanes flying through random turbulence are attenuated by two effects from those that would have been obtained if the angle of attack developed by the gusts encountered along the flight path had been applied directly to the airplane. One of these attenuation effects, called the unsteady lift effect, accounts for the penetration of the gust by the wing and for the buildup of circulation. Investigations into this penetration effect are discussed in references 1 and 2. The other effect, called spanwise averaging, results from the fact that in flight through a random turbulence field there is a variation in the gust-induced angle of attack across the span as well as along the flight path. This investigation is concerned with the latter effect.

A method for calculating the effect of spanwise averaging on the lift, rolling moment, and wing bending moment about the wing root chord of a wing in flight through random turbulence is given in reference 3. This method is applied in reference 4 to a more detailed calculation of the lift for a number of turbulence spectra and for various types of span load distribution. Similar calculations for the rolling moment are given in reference 5.

The data presented in references 3, 4, and 5 are limited to a relatively small number of values of the wing-span parameter β, the ratio of wing span to scale of turbulence, all of which are much larger than those for current airplanes. The minimum value of β for which data are given in reference 4 is 0.25, whereas values for actual airplanes range from 0.03 to 0.15. For this reason, a set of calculations of the lift, rolling moment, and bending moment,

covering a wider range of values of β and encompassing those for current airplanes, was undertaken. Calculations were made for a range of β from 0.001 to 0.250 for both the rectangular and elliptic span load distributions. In performing the calculations, a Dryden power spectral density representation of the turbulence was assumed as the input. A portion of these calculations was used as the basis for a study (ref. 6) which compared the relative magnitudes of the effects of the unsteady lift and spanwise averaging on lift.

The purpose of the present report, therefore, is to make available the full set of results obtained from the calculations of spanwise averaging effects on lift, rolling moment, and root chord bending moment for span ratios covering currently used airplanes, and to compare the results for two span load distributions. The results are presented in the form of plots of the spanwise averaging effect for combinations of nondimensional wing-span and frequency parameters. The data are applicable to unswept wings in incompressible flow.

A parallel set of computations was made for a limited number of span ratios using a Von Karman representation of the turbulence. A comparison of the results for the two input spectral densities is presented in the appendix.

SYMBOLS

The calculations of this investigation were made in the U.S. Customary Units. Both the U.S. Customary and SI Units are presented.

b wing span, m (ft)

F_{bm} span averaging factor for bending moment, $\dfrac{\Phi_{w_e}^{bm}}{\left(\Phi_{w_e}^{bm}\right)_{\beta=min}}$

F_L span averaging factor for lift, $\dfrac{\left(\Phi_{w_e}^{l}\right)_{\beta}}{\left(\Phi_{w_e}^{l}\right)_{\beta=0}}$

F_{rm} span averaging factor for rolling moment, $\dfrac{\Phi_{w_e}^{rm}}{\Phi_{w_e}^{cr}}$

$H_l(k')$ frequency response function of lift due to sinusoidal vertical gust velocity along flight path

$H_{rm}(k')$ frequency response function of rolling moment due to sinusoidal vertical gust velocity along flight path

K taper ratio correction factor

k' nondimensional frequency along span, $\frac{\omega L^*}{U}$

L^* reference scale length of turbulence, assumed 365.76 m (1200 ft)

$\tilde{M}$ bending-moment influence function

$M_1(0)$ $= \eta^*$ for $\eta^* > 0$ and 0 for $\eta^* \leq 0$

$M_2(0,\eta^*)$ $= \eta^*$ for $\eta^* > 0$ and 0 for $\eta^* \geq 0$

r correlation distance between two vertical gust velocities

U velocity along flight path, m/sec (ft/sec)

$\overline{w^2}$ mean square of vertical gust velocity, $(m/sec)^2$ $\left((ft/sec)^2\right)$

y distance along span measured from center line, m (ft)

y^* $= \frac{y}{b/2}$

y'^* nondimensional variable of integration along spanwise direction used only in computing M_1

β wing-span ratio, $\frac{b}{L^*}$

$\gamma(y^*)$ lift or rolling-moment distribution weighting function

η^* nondimensional variable of integration along spanwise direction

ξ $= U\tau$, m (ft)

σ $= \frac{U\tau}{L^*}$

τ time interval between correlation points, sec

$\Phi_{bm}(k')$ power spectral density of bending moment, $(N\text{-}m)^2$ $\left((lb\text{-}ft)^2\right)$

$\Phi_l(k')$ power spectral density of lift, N^2 (lb^2)

$\Phi_{rm}(k')$ power spectral density of rolling moment, $(N\text{-}m)^2$ $\left((lb\text{-}ft)^2\right)$

$\Phi_w(k')$ power spectral density of vertical gust velocity, $(m/sec)^2$ $\left((ft/sec)^2\right)$

$\Phi_{w_e}(k')$ effective power spectral density of vertical gust velocity acting on wing, $(m/sec)^2$ $\left((ft/sec)^2\right)$

$\Phi_{w_e}^{bm}(k')$ effective power spectral density of gust-induced upwash for bending moment, $(m/sec)^2$ $\left((ft/sec)^2\right)$

$\Phi_{w_e}^{cr}(k')$ effective power spectral density of induced upwash assuming a gradient across span equal to maximum gradient for a sinusoidal gust of same amplitude and frequency, $(m/sec)^2$ $\left((ft/sec)^2\right)$

$\Phi_{w_e}^{l}(k')$ effective power spectral density of gust-induced upwash for lift, $(m/sec)^2$ $\left((ft/sec)^2\right)$

$\Phi_{w_e}^{rm}(k')$ effective power spectral density of gust-induced upwash for rolling moment, $(m/sec)^2$ $\left((ft/sec)^2\right)$

$\Psi_w(\ )$ gust correlation function of term in parentheses

$\Psi_{w_e}(L*\sigma)$ effective correlation function of gust influence including wing loading distribution

ω circular frequency, rad/sec

PROCEDURE

The procedure followed in the present work was to adapt the analytical expressions for the power spectra of lift, rolling moment, and bending moment developed in references 3 and 4 for computation on an electronic digital computer. The program included the options for varying the spectrum of turbulence and the wing-span load distribution.

The power spectra were obtained by computing the Fourier transform of the correlation functions for the effective vertical gust velocity (called upwash in ref. 3) on the wing resulting from the influence of turbulence. Since the development of these equations has been presented in references 3 and 4, only those equations necessary for following the work done herein are presented.

Lift Equations Used in Computation

The power spectrum of the lift as described in reference 3 is written here as

$$\Phi_l(k') = \left|H_l(k')\right|^2 \Phi_{w_e}(k') \tag{1}$$

where $H_l(k')$ is the frequency response function relating lift to sinusoidal gust vertical velocities along the flight path and is assumed to be constant across the span. $H_l(k')$ accounts for unsteady lift effects. The term $\Phi_{w_e}(k')$

is an effective power spectral density (PSD) of gust velocity which accounts for the statistical effects of the variations of gust velocity across the span. The term Φ_{w_e} is of primary concern throughout the remainder of the paper, since it is this term that is used to obtain the spanwise averaging effects that are discussed later in the paper.

The expression used to obtain the power spectral density of the effective gust velocity is the Fourier transform of the corresponding correlation function, as expressed by the equation

$$\Phi_{w_e}(k') = \frac{L^*}{U\pi} \int_{-\infty}^{\infty} e^{-k'\sigma} \Psi_{w_e}(L^*\sigma) \, d\sigma \tag{2}$$

The correlation function $\Psi_{w_e}(L^*\sigma)$ is, in turn, given by

$$\Psi_{w_e}(L^*\sigma) = \frac{1}{4} \int_{-1}^{1} \int_{-1}^{1} \gamma\left(y_1^*\right) \gamma\left(y_2^*\right) \Psi_w(r) \, dy_1^* \, dy_2^* \tag{3}$$

where γ is the spanwise lift distribution weighting function and $\Psi_w(r)$ is the gust correlation function.

The factor γ used to describe the spanwise lift distributions is 1 for rectangular loading and $\frac{4}{\pi}\sqrt{1 - y^{*2}}$ for elliptic loading. The following expression for Ψ_w is the correlation function for the Dryden gust distribution:

$$\Psi_w(r) = \overline{w^2}\left(1 - \frac{r}{2L^*}\right)e^{-r/L^*} \tag{4}$$

The quantity r is the correlation distance between two vertical gust velocities in the plane of flight and is obtained by the equation

$$r = \sqrt{(L^*\sigma)^2 + \left(\frac{b}{2}\right)^2\left(y_2^* - y_1^*\right)^2} \tag{5}$$

Flow charts of the programmed computations are shown in figure 1.

Rolling-Moment Equations Used in Computation

The rolling-moment PSD on the wing due to the spanwise gust distribution was obtained by a procedure similar to that for the lift. The only differences

were the terms used for the spanwise distribution weighting functions. For rectangular loading the term was

$$\gamma(y^*) = y^*$$

and for elliptic loading the term was

$$\gamma(y^*) = \frac{4}{\pi} y^* \sqrt{1 - y^{*2}} \tag{6}$$

Bending-Moment Equation Used in Computation

The bending-moment PSD computations followed much the same procedure as for the lift and rolling moment; however, the expression for the gust-correlation function was much more complicated. The development of these expressions is described in greater detail on page 14 of reference 3. The correlation function for the bending moment is

$$\Psi_{w_e} = \frac{1}{b^2} \int_{-1}^{1} \int_{-1}^{1} \tilde{M}\left(y_1^*, \eta_1^*\right) \tilde{M}\left(y_2^*, \eta_2^*\right) \Psi_w(r) \, d\eta_1^* \, d\eta_2^* \tag{7}$$

where $\tilde{M}$ is the bending-moment influence function, and $\Psi_w(r)$ is the same as for the lift cases. The bending-moment influence function is obtained from

$$\tilde{M}(y^*,\eta^*) = \left[(1 - K) \, M_1(y^*) + K \, M_2(y^*,\eta^*)\right] \gamma(\eta^*)$$

where the γ term is the same as that used for lift. The terms $M_1(y^*)$ and $M_2(y^*,\eta^*)$ for the root bending moment are given by

$$M_1(0) = \frac{1}{b} \int_0^1 y^* \, \gamma(y^*) \, dy^*$$

and

$$M_2(0,\eta^*) = \eta^* \quad \text{for} \quad \eta^* > 0$$

$$M_2(0,\eta^*) = 0 \quad \text{for} \quad \eta^* \leq 0$$

The term K is a correction for the effects of wing taper ratio. This term, discussed in reference 5, enters the present calculations only in the case of elliptic loading. In this case, the value is

$$K = \left[C_2 + (C_1 + C_3)\frac{16}{\pi} \int_0^1 \sqrt{1 - y^{*2}}\, y^{*2}\, dy^* \right]^{1/2} \tag{8}$$

The coefficients C_1, C_2, and C_3 are functions of the aspect ratio and were obtained from plots of these coefficients versus a planform parameter presented in reference 7.

COMPUTATIONS AND RESULTS

Computations were made of the effective gust-velocity power spectral density Φ_{w_e} for lift, rolling moment, and bending moment about the root chord. For each of the above factors, the power spectral densities were computed for two span load distributions, rectangular and elliptic, through a range of span ratios β from 0 to 0.25 for lift and 0.001 to 0.25 for both rolling moment and bending moment. The Dryden power spectrum was used as the turbulence input. The magnitude of the mean square of the gust velocity $\overline{w^2}$ was 0.3048 m/sec (1 ft/sec), and the scale of turbulence L^* was assumed to be 365.76 m (1200 ft). In nondimensionalizing the frequency parameter ($k' = \omega L^*/u$) the value for the ratio L^*/u was assumed to be equal to 1.

The results are presented in three groups. The power spectral densities of the effective upwash for the lift for various combinations of β and span load distribution are presented in figures 2 and 3, and a comparison of the normalized data for the two span load distributions is shown in figure 4. Similarly, results for the rolling-moment computations are shown in figures 5 and 6, and the comparison in figure 7. The bending-moment results are shown in figures 8 and 9, and the comparison in figure 10.

The span averaging effect is shown by the normalized power spectral densities for various values of β plotted against a nondimensional span-frequency parameter $k'\beta$. The various power spectral densities have been normalized as follows:

(1) The gust-velocity power spectral density for lift for various values of β was normalized with respect to lift for a span ratio of 0 (gust constant across the span).

$$F_L = \frac{\left(\Phi_{w_e}^{l}\right)_{\beta}}{\left(\Phi_{w_e}^{l}\right)_{\beta=0}}$$

(2) The gust-velocity power spectral density for rolling moment for various values of β was normalized with respect to the case of rolling gusts (sinusoidal gusts with velocity increasing linearly with distance from the center line).

$$F_{rm} = \frac{\Phi_{w_e}^{rm}}{\Phi_{w_e}^{cr}}$$

(3) The gust-velocity power spectral density for bending moment for various values of β was normalized with respect to the minimum β (0.001) for each span load distribution. A span ratio of zero could not be used because the y^* term in the weighting factor causes the bending moment to go to zero.

$$F_{bm} = \frac{\Phi_{w_e}^{bm}}{\left(\Phi_{w_e}^{bm}\right)_{\beta=min}}$$

The comparisons for the two span load distributions are made for the same total lift for the two loadings. It is assumed that the lift is proportional to the wing area; then, for the same wing span, the aspect ratio will be the same.

DISCUSSION

Lift

The effect of span ratio on the lift gust power spectral densities $\Phi_{w_e}^{l}$ for the two span loadings is shown in figures 2 and 3. The pattern of the data for various span ratios is essentially the same for both conditions; the values differ only slightly in magnitude.

The effect of span ratio on averaging out gust angles of attack can also be seen in figures 2(a) and 3(a) by the decreasing value of the power spectra with an increase in span ratio, which is heightened with increasing frequency (decreasing wavelength). This effect of span ratio is shown directly on the cross plots presented in figures 2(b) and 3(b). For small frequencies (long wavelengths), the effect of span ratio is negligible because both the large and small wings are immersed more or less in a similar gust field. However, as the frequency increases (the turbulence wavelength decreases) or the wing span increases the wing is affected more and more by the randomness of the turbulence fields.

The data shown in figures 2(c) and 3(c) are the ratios of the effective gust-velocity power spectral densities for the various values of β normalized with respect to the power spectra for $\beta = 0$ (gust spectrum) at each frequency plotted against a factor $k'\beta$, which is a nondimensional frequency based on wing span $\omega b/U$. Figures 2(d) and 3(d) are merely expansions of the upper left corners of figures 2(c) and 3(c) to obtain a better separation of the curves in the region.

Figures (2(c) and 3(c)) show that, except for very low values of $k'\beta$, the data for various values of the span ratio fall on a single curve. This curve represents the attenuation of lift due to the spanwise averaging effect as a function of reduced frequency. In reference 6, these data are compared with the attenuation of lift as a function of frequency caused by unsteady lift effects. At very low values of $k'\beta$, figures 2(d) and 3(d), there is a decrease in the ratio of the gust power spectral densities with increasing size. This is believed to be due, as explained in reference 6, to the probability of occasionally encountering a gust which is not uniform across the span. This, of course, is more likely to occur with a larger wing than with a smaller wing since a larger portion of the atmosphere is encountered.

A comparison of the attenuations due to the spanwise averaging effect for elliptic and rectangular wings is shown in figure (4). This comparison shows that the elliptic span distribution has somewhat less attenuation than the rectangular span distribution. This result should be expected, since for the elliptic wing a larger portion of the total lift is distributed inboard toward the center of the wing, causing it to behave like a slightly smaller wing.

As an example of the attenuations effect, due to span averaging, on the lift and thus on the normal acceleration of an airplane resulting from gust-induced angles of attack, consider the response of an airplane at about 1 Hz. Motion at this frequency is very bothersome to the passengers and, unfortunately, both the gust energy and the response of the airplane generally are high also. For a specific example, consider a typical moderate size transport, $b = 45.72$ m (150 ft) and $U = 223.52$ m/sec (733.33 ft/sec), for which the value of $k'\beta$ would be 1.28. From figure 4 the ratio of the power spectral densities for the elliptic span distributions is about 0.86. Since the lift is proportional to the square root of the power spectral density, the reduction in the lift increment due to a constant angle of attack by the span averaging can be obtained from the expression $1 - \sqrt{F_L}$. For the airplane described above, this reduction is about 7 percent.

Rolling Moment

The power spectral densities of the effective gust-induced angle of attack for the rolling moment $\Phi_{w_e}^{rm}$ for the rectangular and elliptic wings are presented in figures 5 and 6, respectively. For the rolling moment, as for the lift, the patterns of variations for the rectangular and elliptic loadings are similar with only minor differences for the various conditions. As would be expected, the variations of the spectra with frequency parameter k' are similar to

those presented in reference 3. The difference between the values presented in this report and those in reference 3 is due to the different factors used for normalization.

The ratio of the PSD of the effective rolling moment due to gusts to that for a wing subjected to sinusoidal rolling gusts is shown in figures 5(c) and 6(c). The magnitude of the rolling gust at each frequency corresponds to the assumption that the gradient across the span is equal to the maximum gradient of gust velocity with distance for a sinusoidal gust of the same amplitude and frequency. It is immediately apparent that, in contrast to the case for lift, the values for this ratio are very small for all the values of $k'\beta$. This result indicates that the rolling moments generated by flight through the random gust field are much lower than those for the assumed rolling gusts. The highest values of the ratio occur at the higher values of $k'\beta$, where randomness of the gusts tends to introduce an uneven angle-of-attack pattern with some resultant rolling moment. At the low values of $k'\beta$, which represent small wings or long wavelengths, the value of the ratio is lowest since, for these situations, the wing is more likely to be immersed in a more nearly uniform field; therefore, there is little rolling moment.

A comparison of the spanwise averaging effect on the rolling moment for the two loading conditions is shown in figure 7 for three representative wing-span ratios. The ratios of power spectral densities are slightly lower for the elliptic lift distribution than for the rectangular. Both sets of data were normalized by the same quantities (steady rolling representation) and, since the rectangular loading has a loading representation closely resembling the normalizing term, its ratio shows directly the effect of span averaging. The elliptic loading, because of its modification of the load shape, results in a shorter moment arm and, thus, less rolling moment for a comparable value of $k'\beta$ than does the rectangular loading.

Bending Moment

The power spectral densities for the effective gust velocity for the bending moment about the root chord are presented in figures 8 and 9. The pattern of the power spectral density for the bending moment closely resembles that of the lift, since the bending moment is proportional to the lift function on the free semispan.

The difference in magnitude of the effective power spectral densities between the elliptic and rectangular lift distributions is probably due to the relative inward loading for the elliptic distribution, discussed previously, which results in a shorter effective moment arm.

The spanwise averaging effect shown in figures 8(c) and 9(c) is, again, similar to that for the lift cases. The bending-moment ratio shown is that for $\left(\Phi_{w_e}^{bm}\right)_\beta \Big/ \left(\Phi_{w_e}^{bm}\right)_{\beta=min}$ where $\left(\Phi_{w_e}^{bm}\right)_{\beta=min}$ is that for the smallest, other than zero, span considered ($\beta_{min} = 0.001$). Zero span could not be used since the moment has a term proportional to the span; thus, the power spectral density

would be zero at zero span. At high enough values of $k'\beta$, the averaging effect decreased the power spectral density to about 30 percent of that for the low values. The bending moment attenuation, which is proportional to the square root of the power spectral density attenuation, reduced the value to about 55 percent. The expansion of the curves at low values of $k'\beta$ in figures 8(d) and 9(d) shows a similar effect to that displayed by the lift power spectral densities; that is, for the large wing spans the ratios did not reach all the way up to 1.0. This decrease probably occurs for the same reason, in that a large wing sampling a larger portion of the atmosphere is more likely to encounter a patch of irregular gust distribution with a consequent reduction in overall load. A comparison of the power spectral densities for the effective gust velocities for bending moments is shown in figure 10 for the two span load distributions. Thus, some of the effect of the span load distributions was absorbed in the normalization procedure because the data for $\beta = 0.001$ contain some of the span load effect; if it were possible to use $\beta = 0$ for normalization, the difference between the curves might be somewhat greater. However, there is still some effect of the span loading shape, as exemplified by the somewhat greater attenuation for rectangular loading than for the elliptic loading. The reason for this is similar to that for lift case, in that for the elliptically loaded wing, its relatively higher inboard loading causes it to behave like a somewhat smaller wing.

Von Karman Turbulence Representation

The results of computations made using the Von Karman turbulence representations were very similar to those for the Dryden representation and, consequently, complete data are not presented. A comparison of the results for the two input spectral densities is presented in the appendix.

CONCLUDING REMARKS

The effective power spectral densities of the gust input to the lift, rolling moment, and root chord bending moment of wings of various spans as a result of random turbulence input were computed. The input turbulence was represented by the Dryden power spectral density and the ratios of wing span to scale of turbulence encompassed the range of current airplanes. The wing spans are presented as ratios of the span to the scale of turbulence.

The results developed in this investigation are presented primarily to provide data on the span averaging effect for wing-span ratios encompassing current airplane sizes, and to provide a comparison between elliptic and rectangular span load distributions.

The results for the lift computations showed that the averaging effect of the wing span was increased with both wing span and the inverse of the turbulence characteristic wavelength. As a result of this lift averaging effect, the lift load on a wing and consequently the normal acceleration of a typical passenger airplane due to random turbulence in the frequency range most bothersome to passengers can be about 7 percent less than the load indicated by considering the turbulence-induced angle of attack constant across the span. The

effects for both elliptic and rectangular span load distributions were similar, with the rectangular distribution showing a slightly (4 percent) greater averaging effect.

The root chord bending moment, since it is directly related to the lift loading, shows a spanwise averaging effect similar to that for the lift. However, it is somewhat smaller, showing only a 2-percent decrease in the bending moment over that which might be expected when the turbulence-induced angle of attack is considered constant. The effects for both an elliptic span load distribution and rectangular distribution are similar with the rectangular distribution showing a slightly (1 percent) greater averaging effect.

The rolling-moment span averaging effect was opposite to that for the lift or bending moment. Most of the effect occurred at the longer wavelengths rather than at the shorter wavelengths.

Using the Von Karman turbulence representation instead of the Dryden had only a minor effect on the results. The pattern of the data was the same and the magnitude differed only slightly. The span averaging effect on the lift and root chord bending moment was slightly greater for the Von Karman data (about 2 to 3 percent) than for the Dryden data. The rolling moments for the Von Karman spectrum were slightly larger.

Langley Research Center
National Aeronautics and Space Administration
Hampton, VA 23665
July 6, 1978

APPENDIX

SPAN AVERAGING EFFECTS USING A VON KARMAN REPRESENTATION OF THE TURBULENCE

A set of span averaging effects similar to those for the Dryden turbulence representation discussed in the main body of the report, but using the Von Karman representation of the turbulence, were made for both rectangular and elliptic span load distributions. The computational procedure was parallel for the two sets of data and therefore is not repeated; the difference consisted of substituting the following correlation function for the Von Karman gust distribution:

$$\psi_w(r) = \overline{w^2}(0.59253)^3 \sqrt{\frac{r}{1.339}}\left[K_{1/3}\left(\frac{r}{1.339}\right) - \frac{r}{2(1.339)} K_{2/3}\left(\frac{r}{1.339}\right)\right] \quad \text{(A1)}$$

for the Dryden function in equation (4).

The terms $K_{1/3}\left(\frac{r}{1.339}\right)$ and $K_{2/3}\left(\frac{r}{1.339}\right)$ in the Von Karman correlation function are modified Bessell functions of the second kind of argument $\left(\frac{r}{1.339}\right)$ and order 1/3 and 2/3, respectively.

The computations for the Von Karman data were made for only 5 span ratios (β = 0.0, 0.031, 0.063, 0.125, and 0.250) rather than the 10 for the Dryden because the Bessel function computations increased the computer run time by more than a factor of 5.

The results of the computations using the Von Karman gust representation were very similar to those obtained for the Dryden representation, differing only by a relatively small magnitude. A presentation of the entire body of data was not, therefore, considered necessary. However, figures showing comparisons for the two turbulence representations are presented.

A comparison of the two input turbulence spectral densities is shown in figure 11.

The comparisons of the effective gust power spectral density for lift for the four conditions - elliptic and rectangular span load distributions for both the Dryden and Von Karman gust representations - are shown in figure 12. The span averaging effect obtained when the Von Karman representation of the turbulence field was used was slightly greater than when the Dryden representation was used. For the example airplane discussed in the main body of the text, this increase in span averaging effect was about 3 percent (10 percent compared with 7 percent). This result is in agreement with the results discussed in reference 8 where only the acceleration was considered and where it was mentioned that the normal acceleration weighting factor was somewhat less for the Von Karman than for the Dryden representation.

APPENDIX

The comparisons of the effective gust inputs for the root chord bending moment for the four conditions are presented in figure 13. Here, as in the case of the lift, the Von Karman data showed a slightly greater span averaging effect than the Dryden data (4 percent compared with 2 percent for the same airplane example).

The comparisons of the effective gust inputs for the rolling moments for the four conditions are shown in figure 14. The comparison here showed that the Von Karman representation of the turbulence resulted in slightly greater rolling disturbances than did the Dryden representation.

REFERENCES

1. Küssner, H. G.: Zusammenfassender Bericht über den instationären auftrieb von Flügeln. Luftfahrt-forschung, Bd. 13, Nr. 12, Dec. 20, 1936, pp. 410-424.

2. Jones, Robert T.: The Unsteady Lift of a Wing of Finite Aspect Ratio. NACA Rep. 681, 1940.

3. Diederich, Franklin W.: The Response of an Airplane to Random Atmospheric Disturbances. NACA Rep. 1345, 1958.

4. Diederich, Franklin W.; and Drischler, Joseph A.: Effect of Spanwise Variations in Gust Intensity on the Lift Due to Atmospheric Turbulence. NACA TN 3920, 1957.

5. Eggleston, John M.; and Diederich, Franklin W.: Theoretical Calculation of the Power Spectra of the Rolling and Yawing Moments on a Wing in Random Turbulence. NACA Rep. 1321, 1957.

6. Phillips, William H.; and Lichtenstein, Jacob H.: Comparison of Effects of Unsteady Lift and Spanwise Averaging in Flight Through Turbulence. NASA TM X-74028, 1977.

7. Diederich, Franklin W.: A Simple Approximate Method for Calculating Spanwise Lift Distributions and Aerodynamic Influence Coefficients at Subsonic Speeds. NACA TN 2751, 1952.

8. Pratt, Kermit G.: Effect of Spanwise Variation of Turbulence on the Normal Acceleration of Airplanes With Small Span Relative to Turbulence Scale. NASA TM X-72748, 1975.

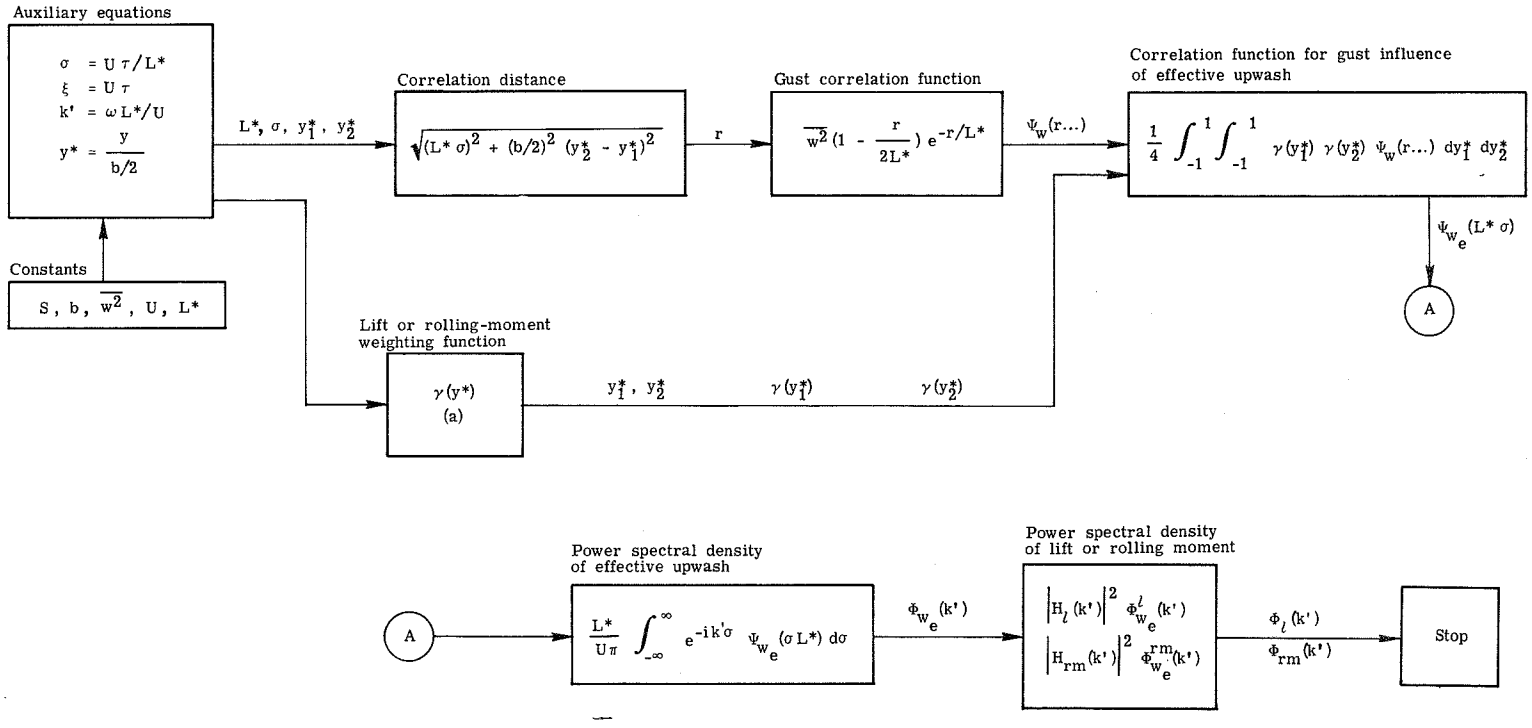

[a] Weighting functions for span loading

Response	Rectangular	Elliptical
Lift	1	$\frac{4}{\pi}\sqrt{1 - y^{*2}}$
Rolling moment	y^*	$\frac{4}{\pi} y^* \sqrt{1 - y^{*2}}$

(a) Lift and rolling moment.

Figure 1.- Flow charts of computation program for investigation.

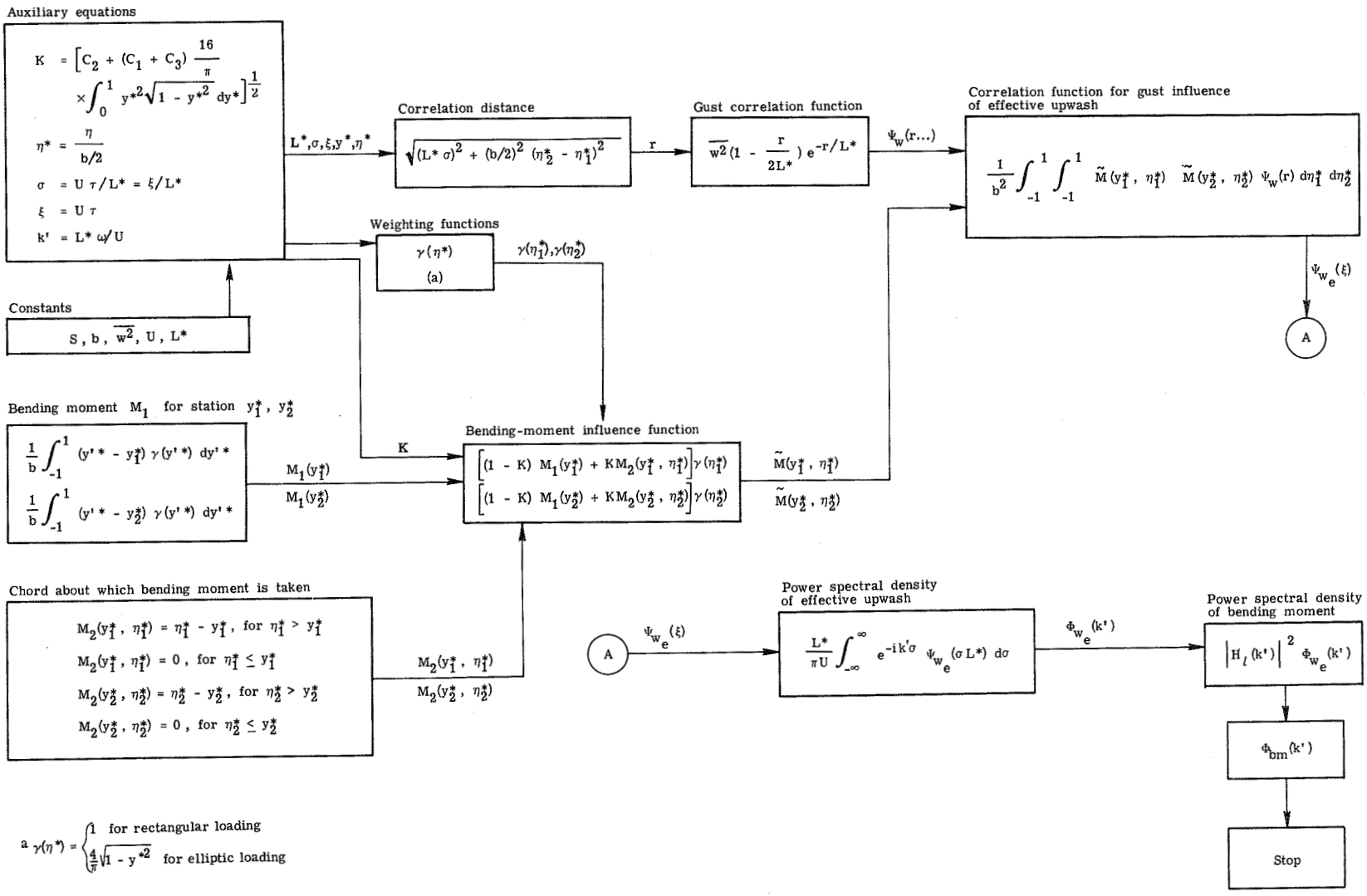

(b) Bending moment.

Figure 1.- Concluded.

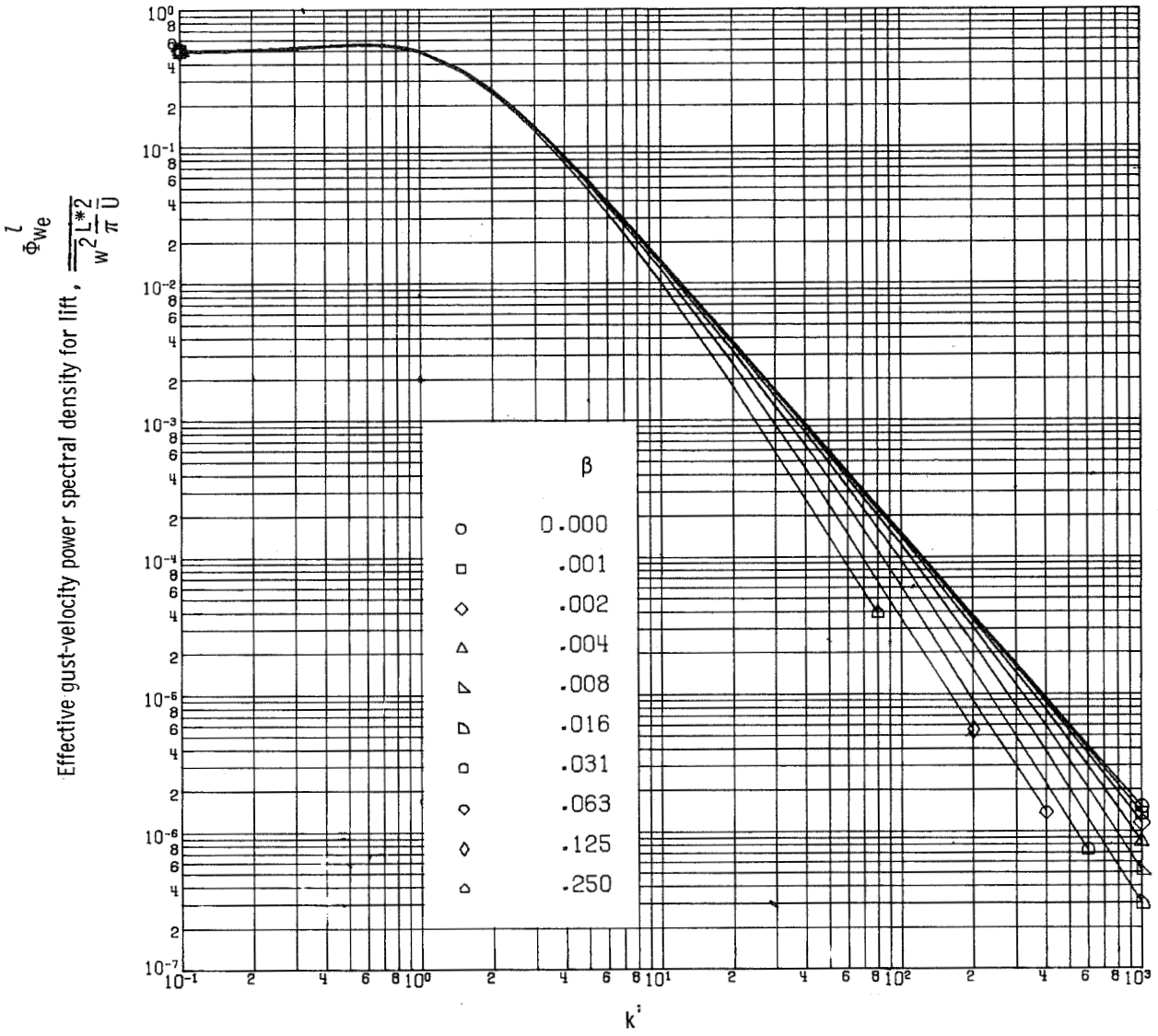

(a) Effective power spectral density plotted against nondimensional frequency for various span ratios.

Figure 2.- Effective gust-velocity power spectral densities for lift computed for rectangular span load distribution and a range of wing-span ratios.

The curves have been nondimensionalized for $\overline{w^2}$ = 0.3048 m/sec (1 ft/sec) and L* = 365.76 m (1200 ft).

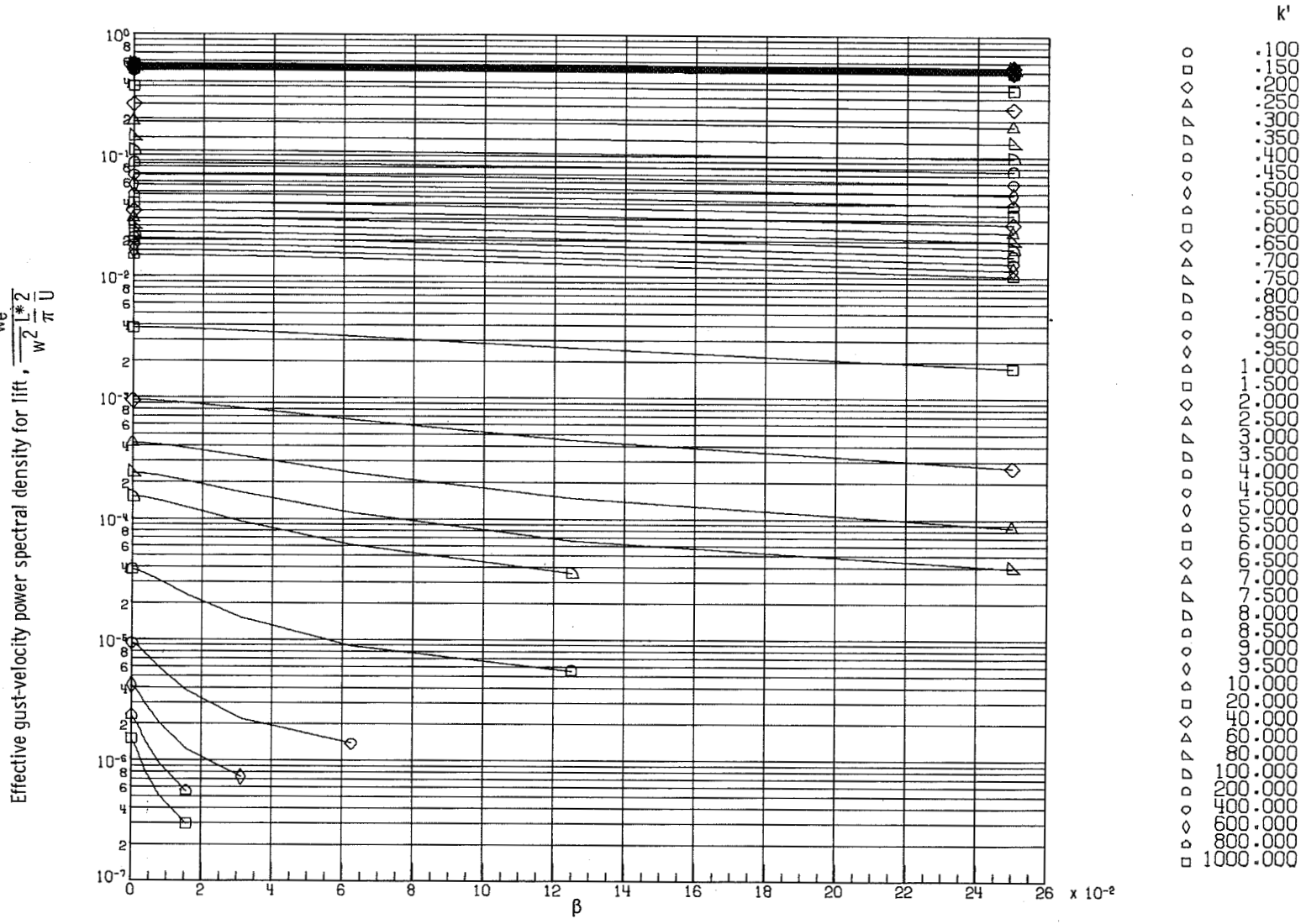

(b) Effective power spectral density plotted against wing-span ratio.

Figure 2.- Continued.

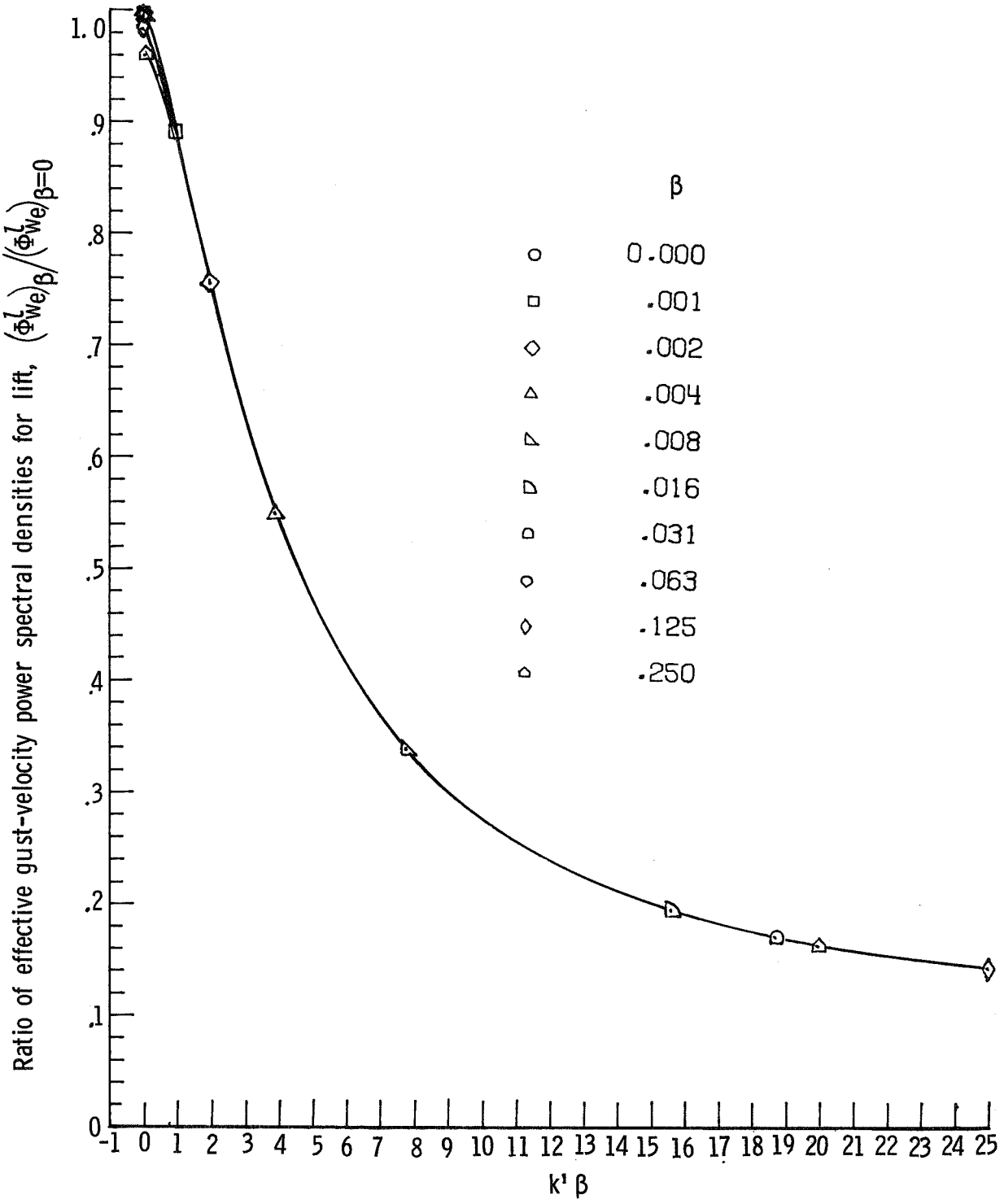

(c) Ratio of effective power spectral densities for various span ratios to that for zero span ratio.

Figure 2.- Continued.

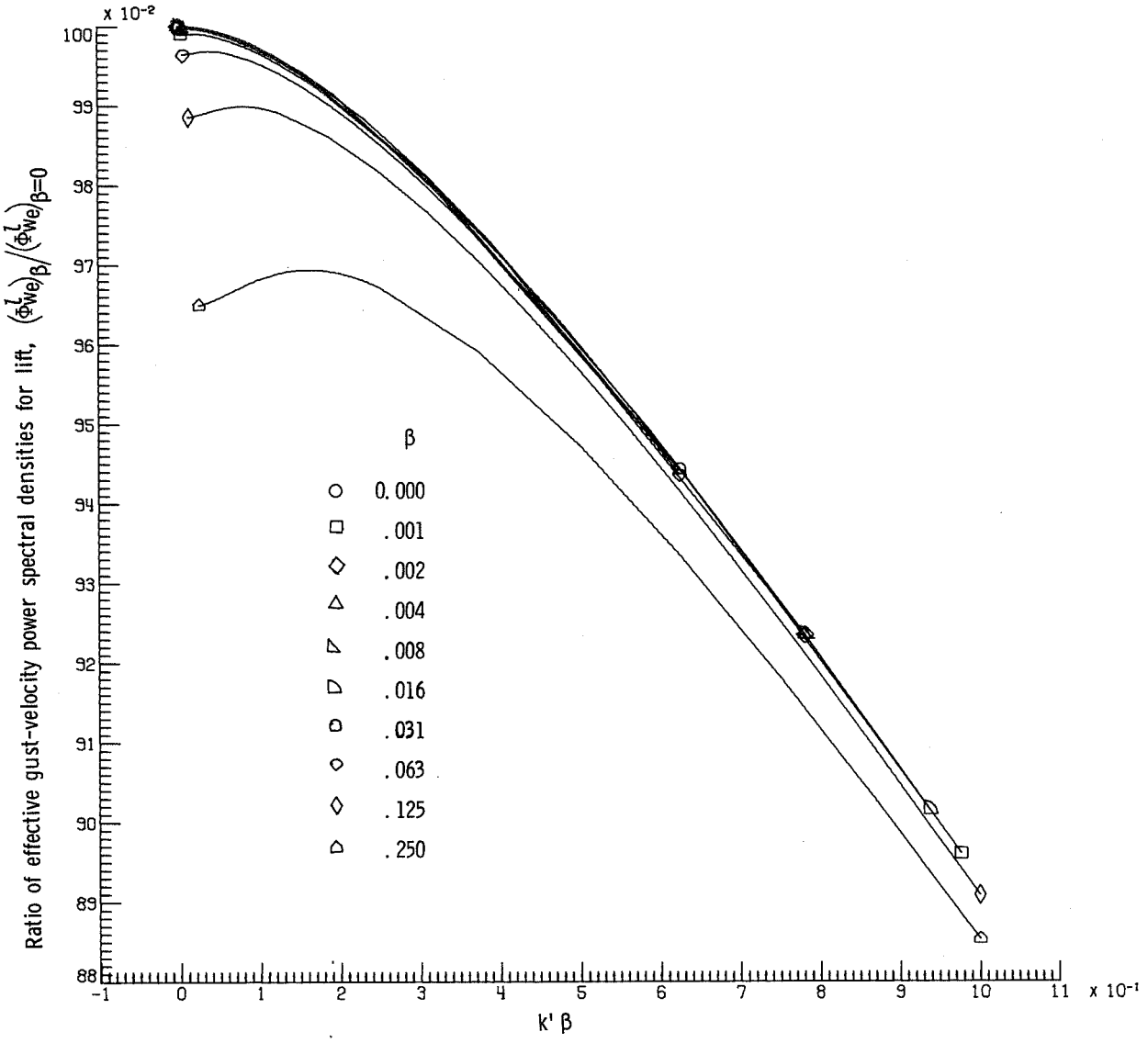

(d) Ratio of effective power spectral densities for various span ratios to that for zero span ratio. Expansion of upper left corner of figure 2(c).

Figure 2.- Concluded.

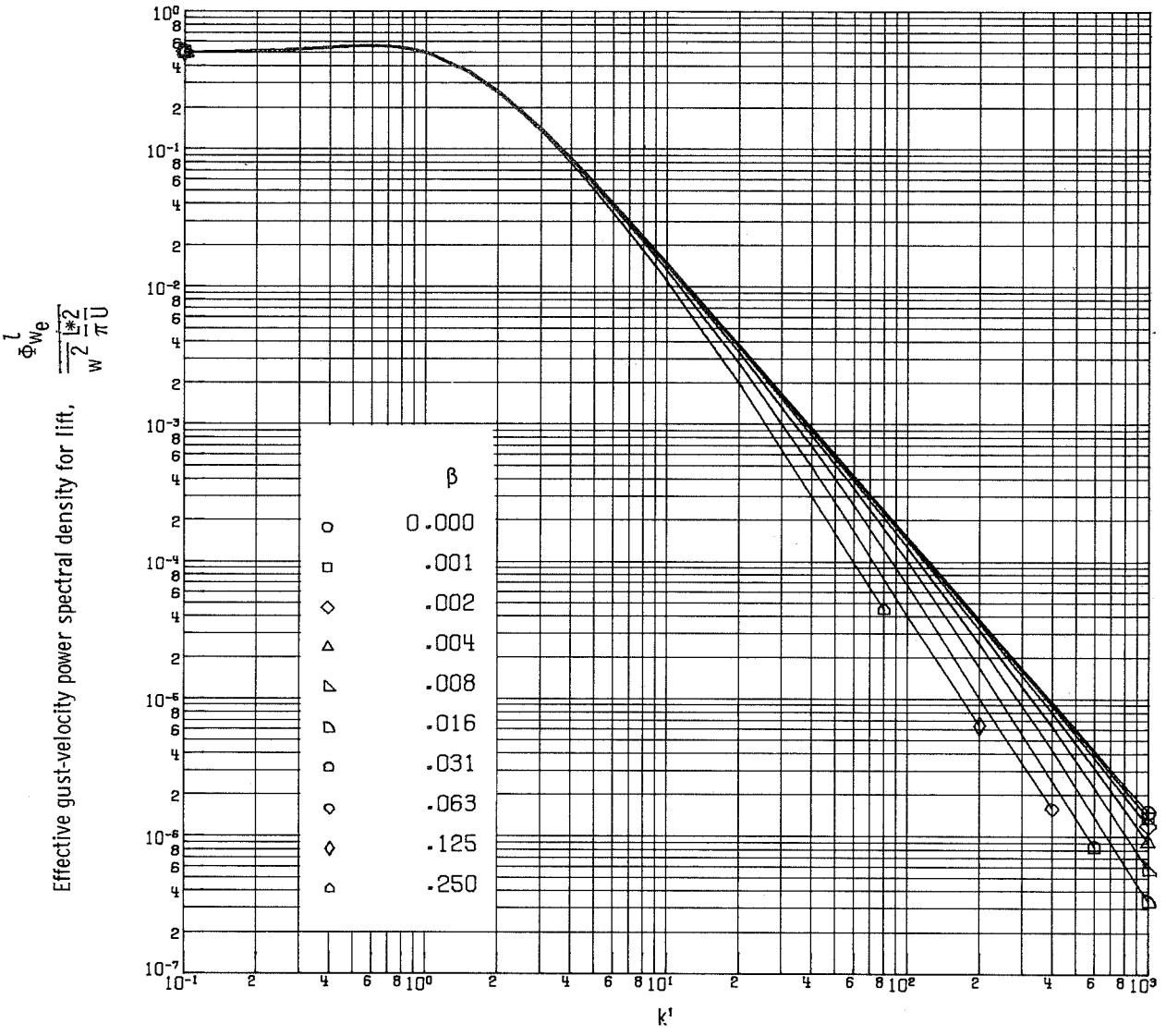

(a) Effective power spectral density plotted against nondimensional frequency for various span ratios.

Figure 3.- Effective gust-velocity power spectral densities for lift computed for elliptic span load distribution and a range of wing-span ratios. The curves have been nondimensionalized for $\overline{w^2}$ = 0.3048 m/sec (1 ft/sec) and L* = 365.76 m (1200 ft).

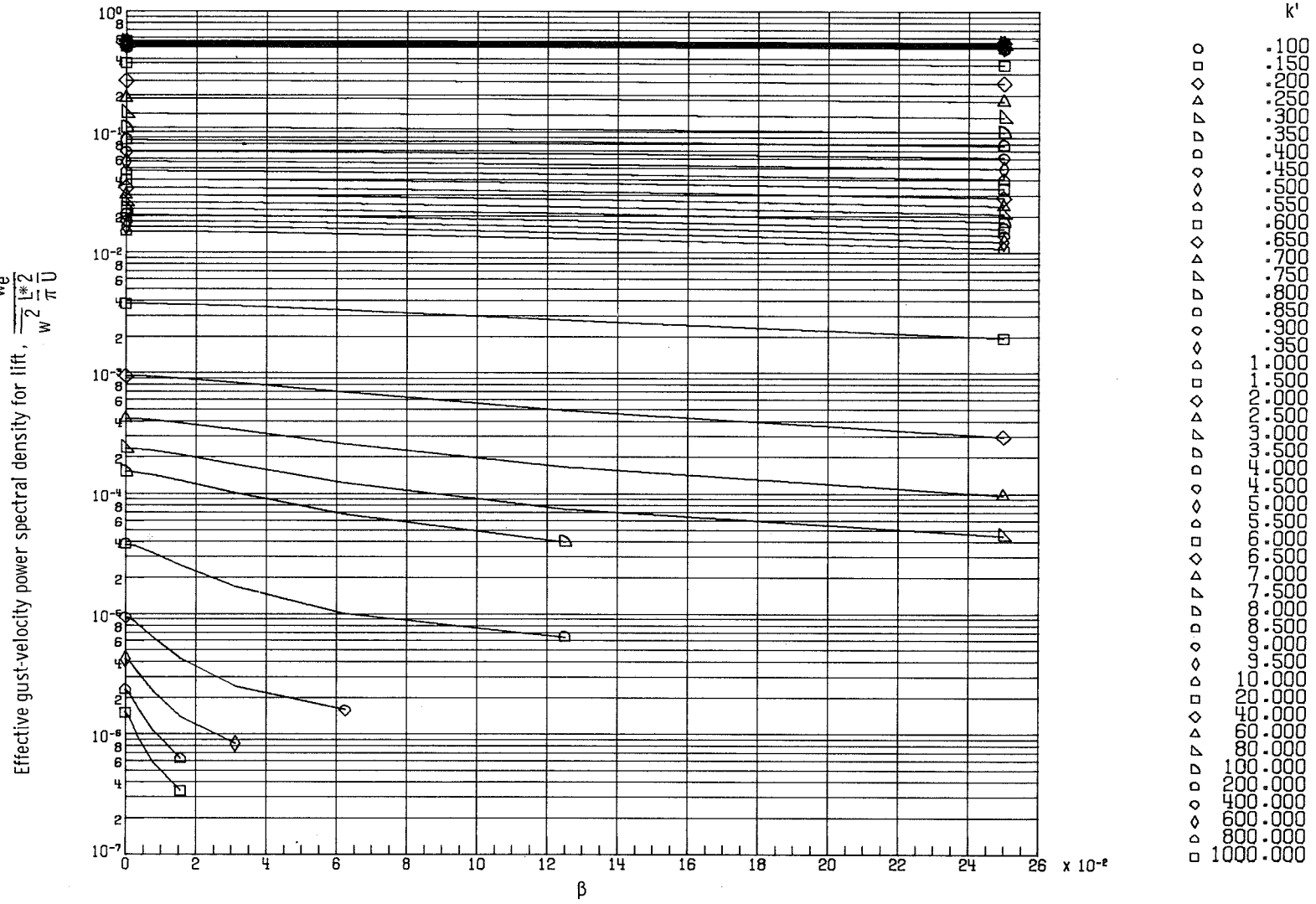

(b) Effective power spectral density plotted against wing-span ratio.

Figure 3.- Continued.

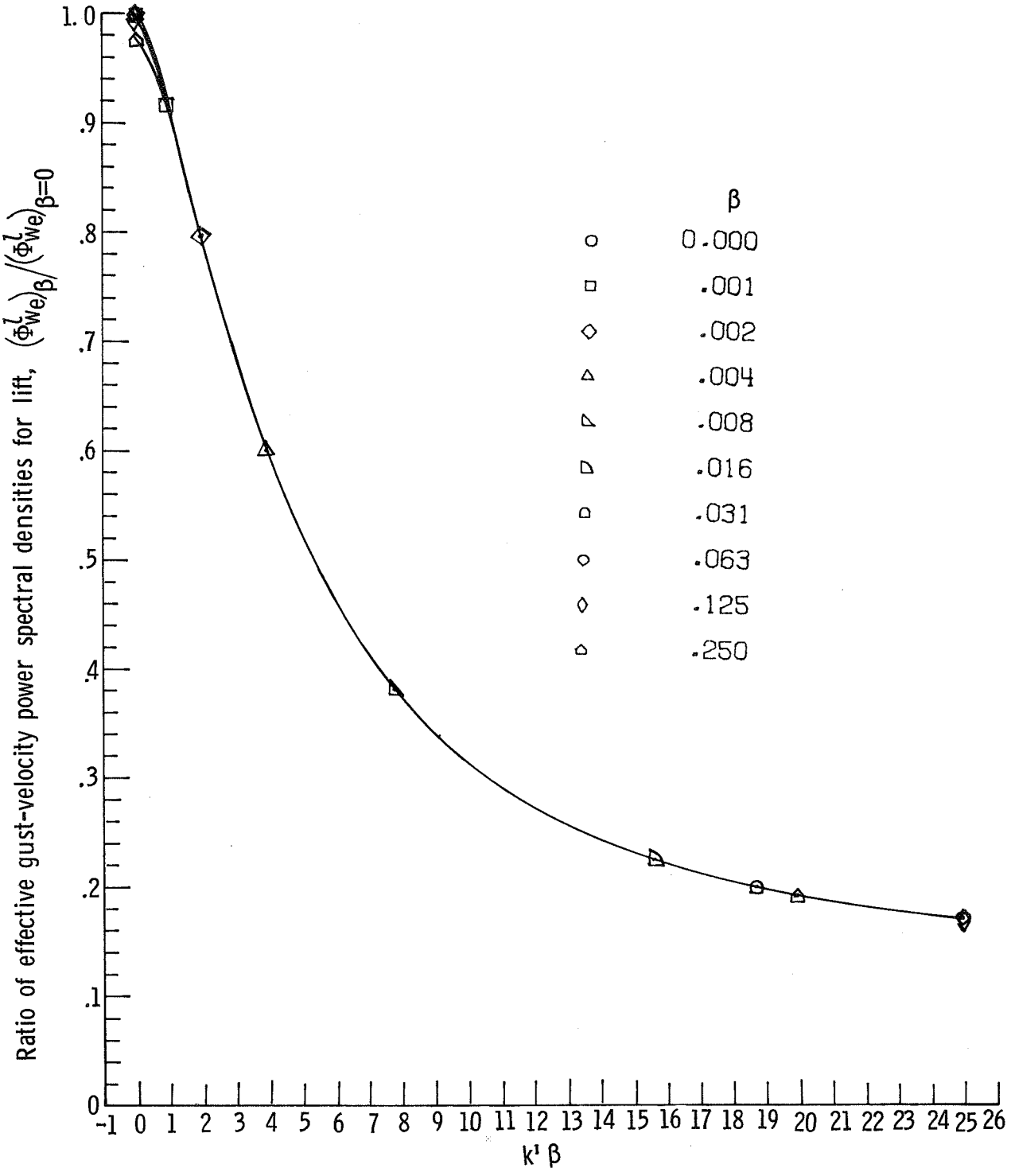

(c) Ratio of effective power spectral densities for various span ratios to that for zero span ratio.

Figure 3.- Continued.

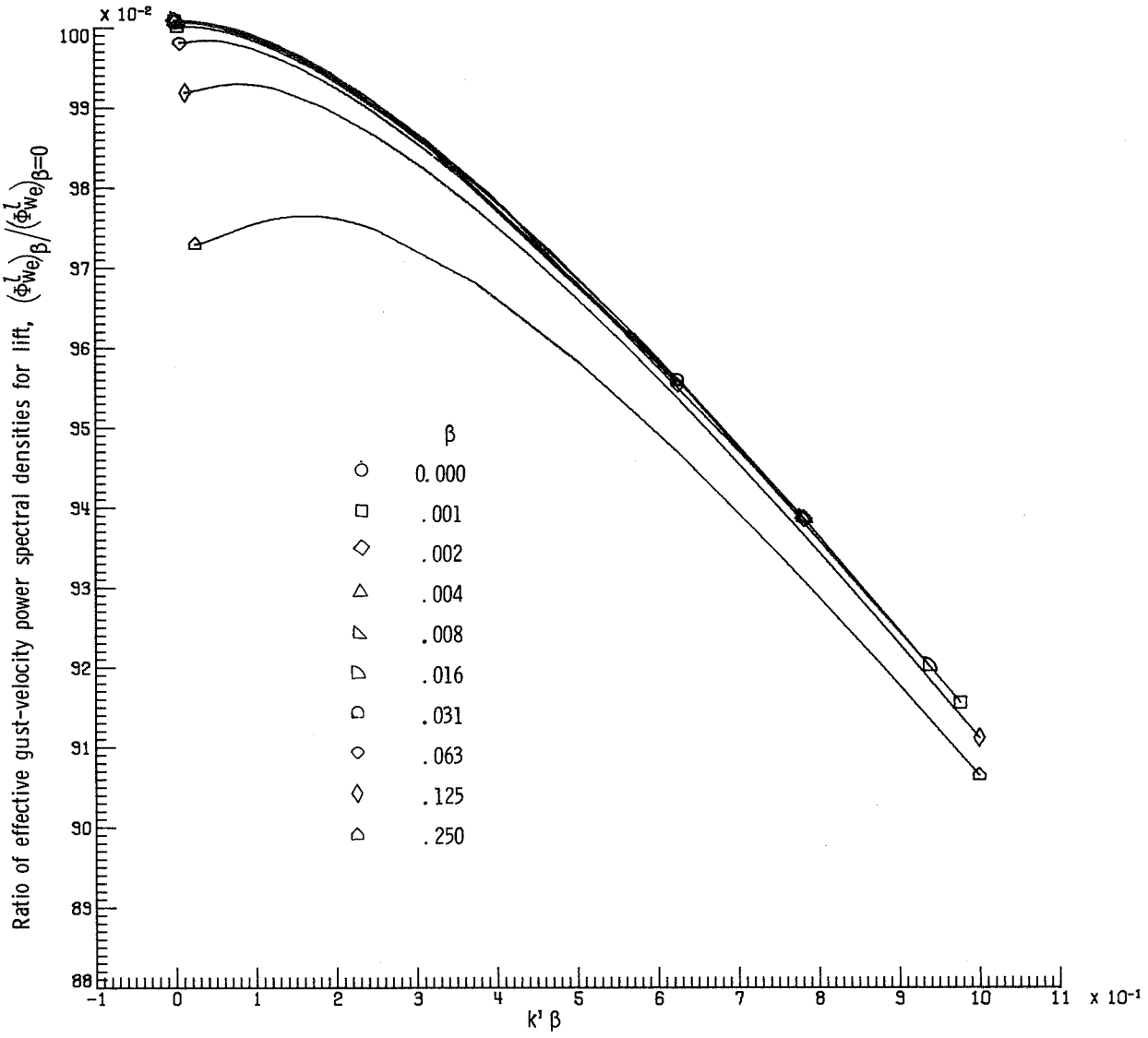

(d) Ratio of effective power spectral densities for various span ratios to that for zero span ratio. Expansion of upper left corner of figure 3(c).

Figure 3.- Concluded.

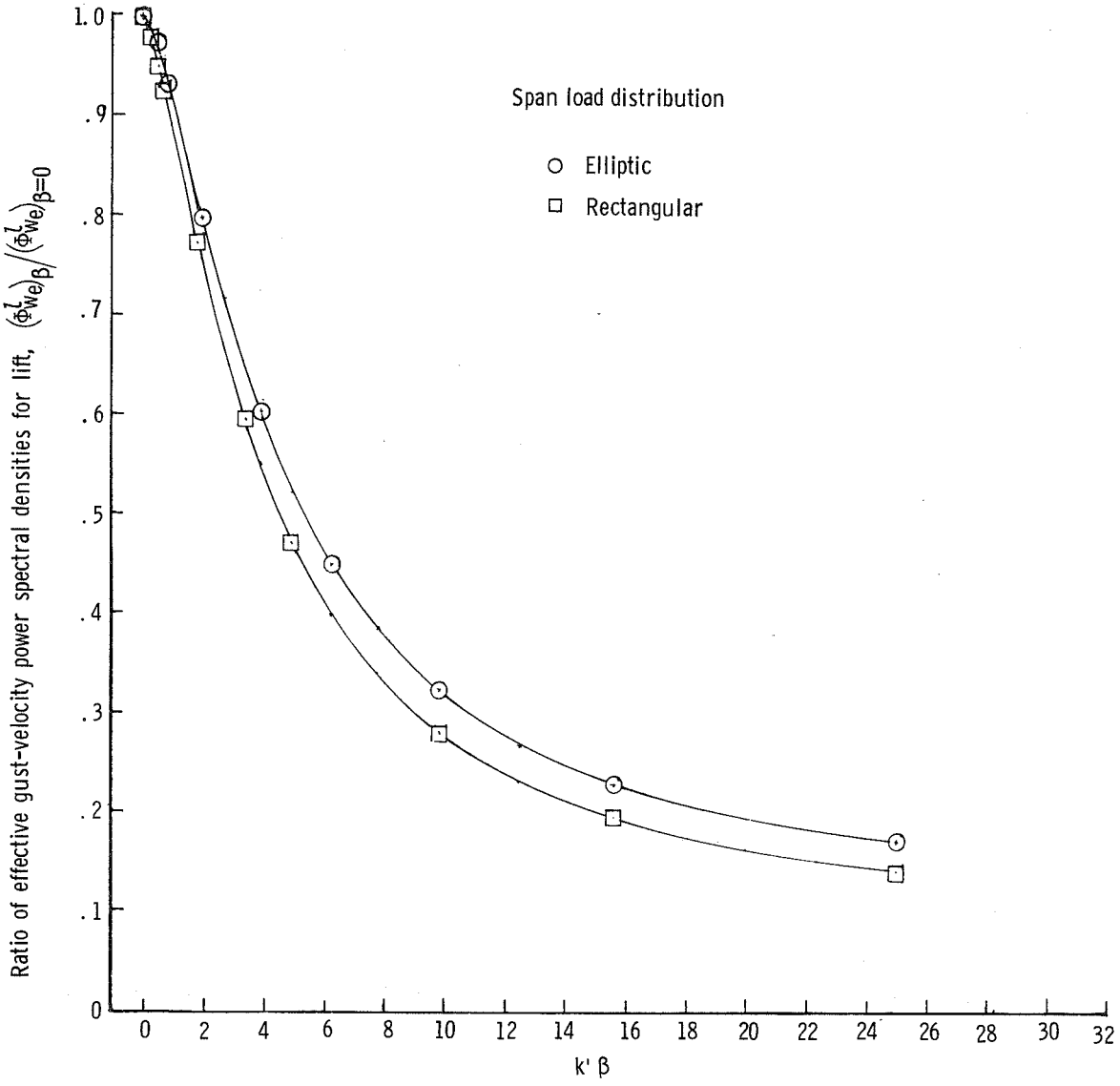

Figure 4.- Comparison of wing-span averaging effect on effective gust power spectral density for lift between rectangular and elliptic span load distributions.

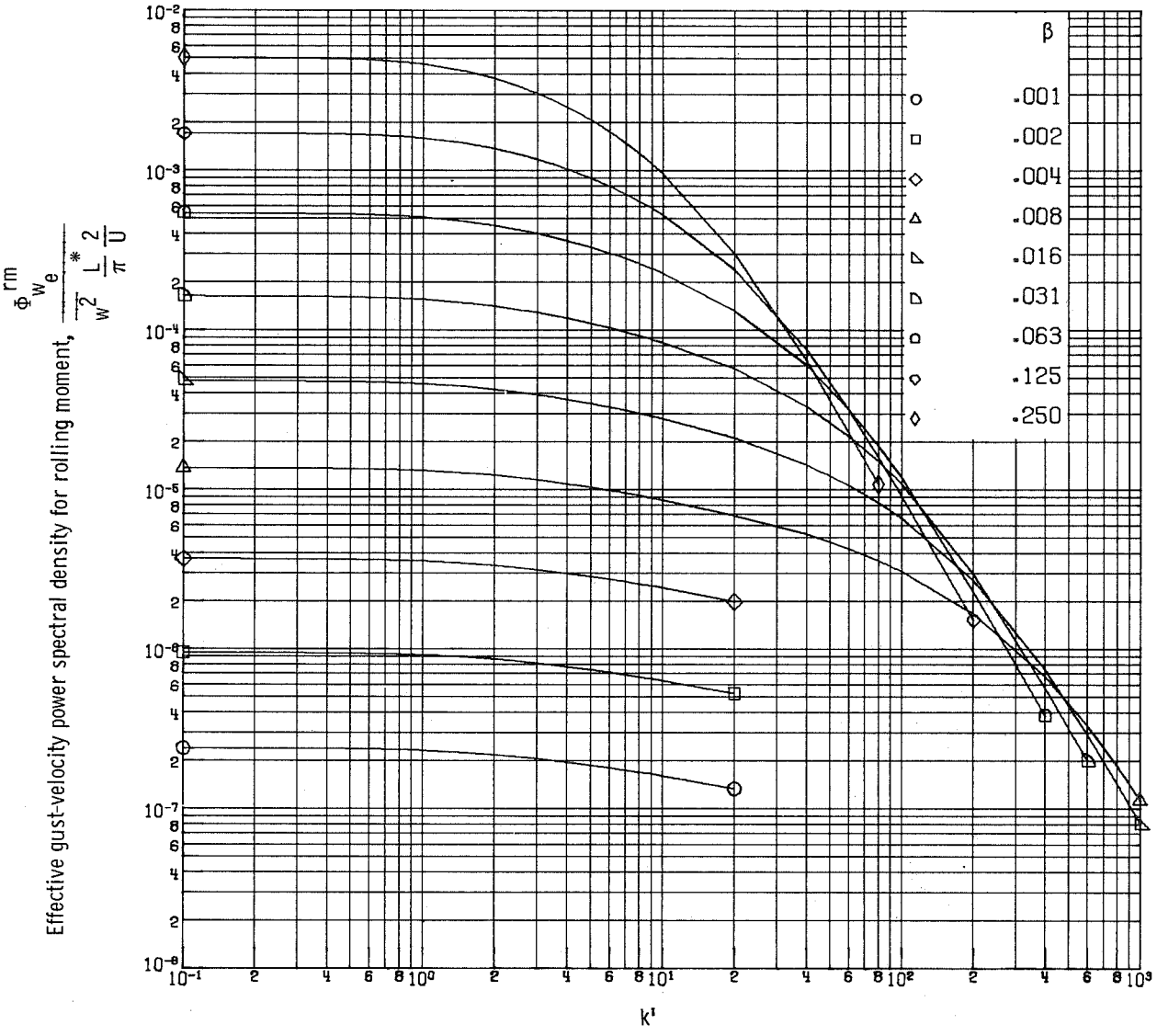

(a) Effective power spectral density plotted against nondimensional frequency for various span ratios.

Figure 5.- Effective gust-velocity power spectral densities for rolling moment computed for rectangular span load distribution and a range of wing-span ratios. The curves have been nondimensionalized for $\overline{w^2}$ = 0.3048 m/sec (1 ft/sec) and L* = 365.76 m (1200 ft).

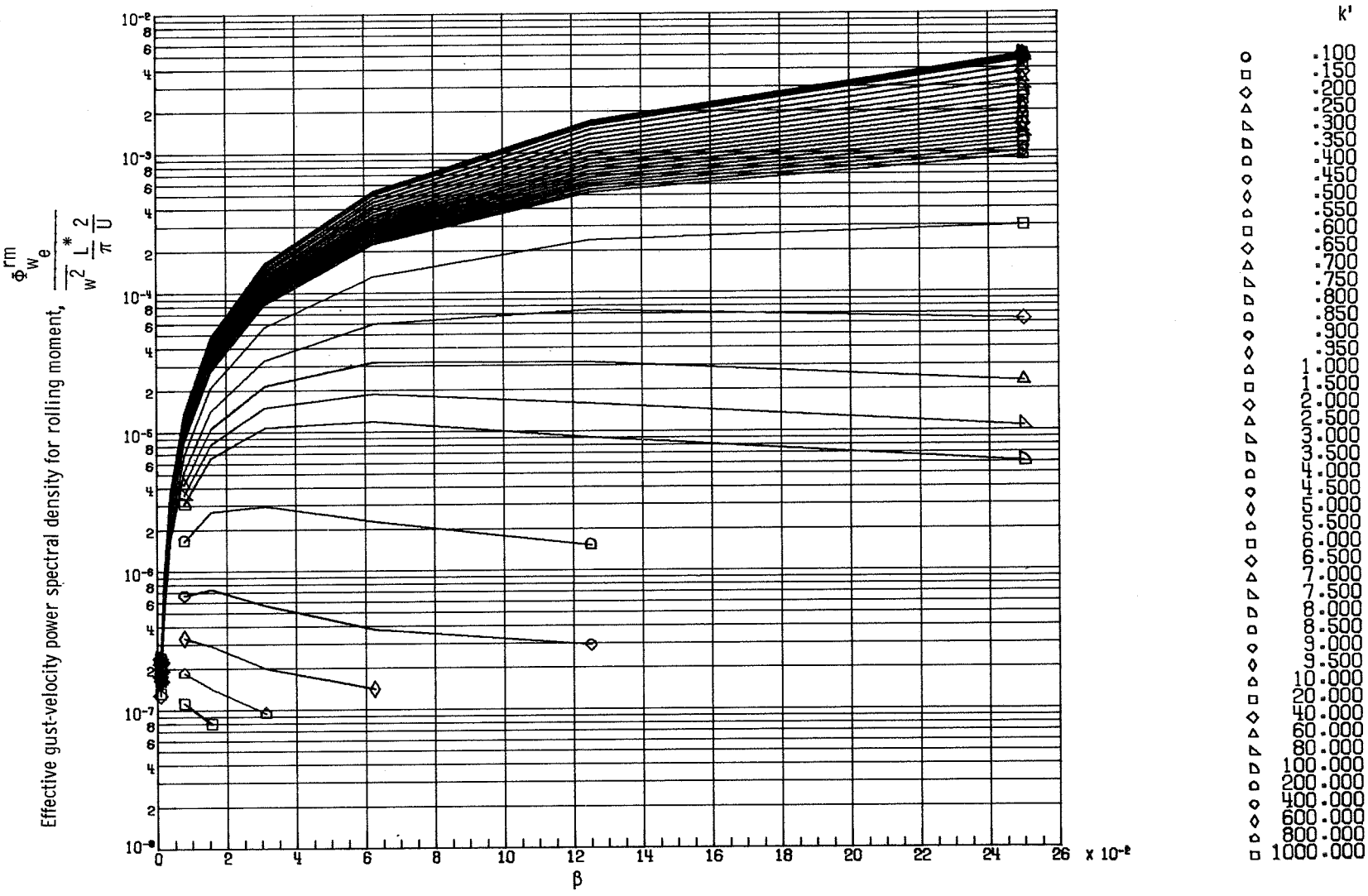

(b) Effective power spectral density plotted against wing-span ratio.

Figure 5.- Continued.

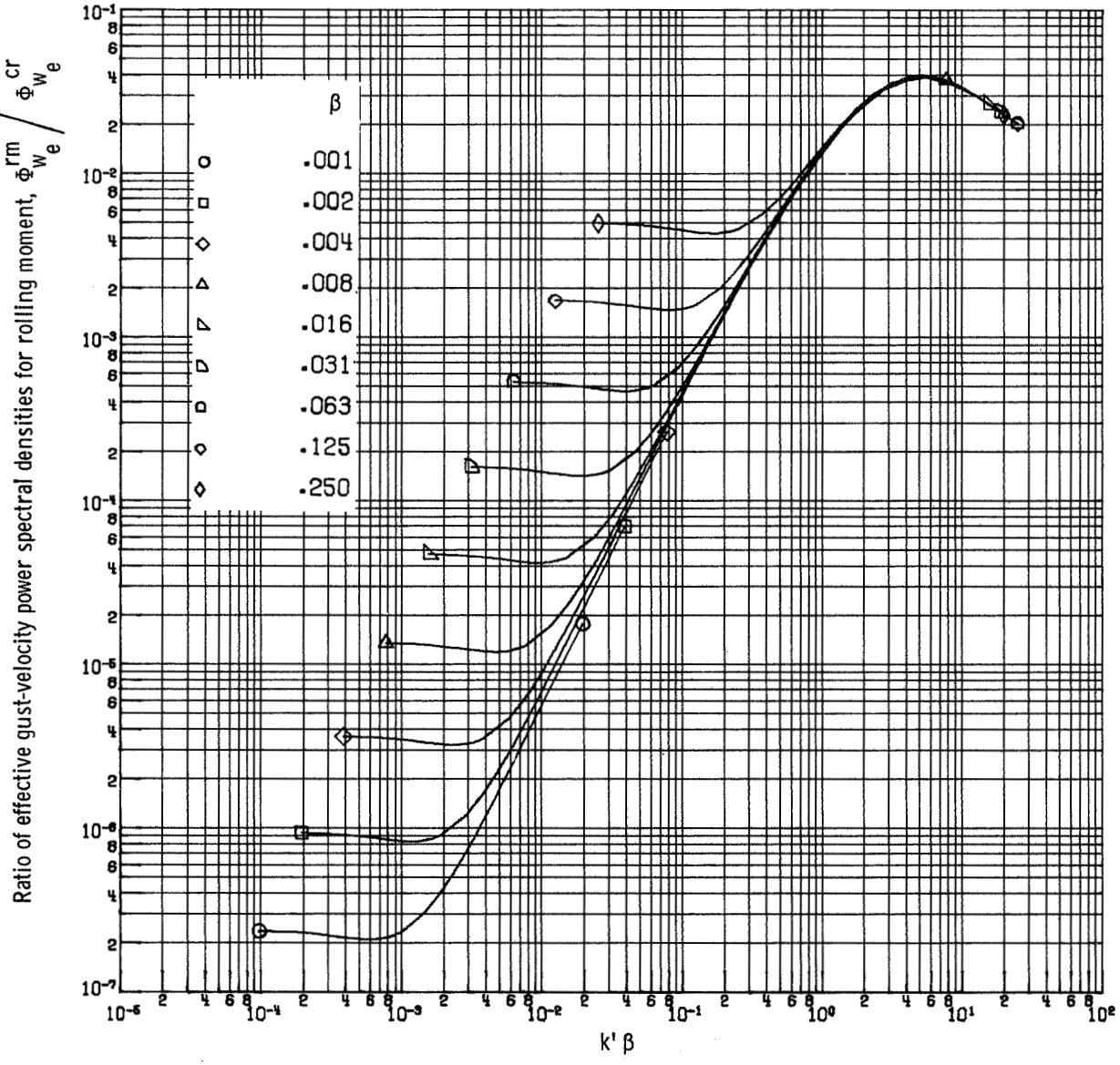

(c) Ratio of effective power spectral densities for various span ratios to that for steady rolling.

Figure 5.- Concluded.

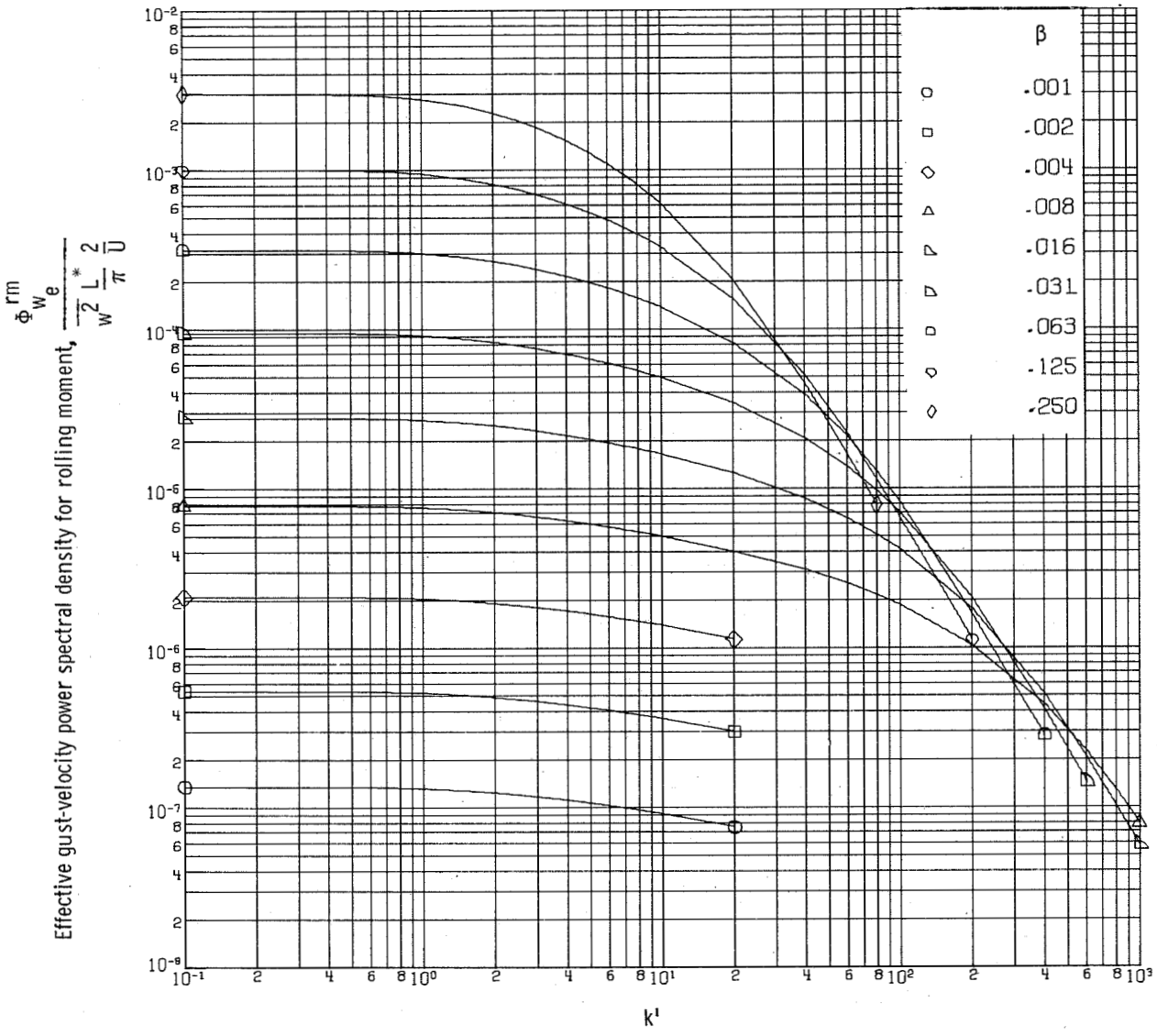

(a) Effective power spectral density plotted against nondimensional frequency for various span ratios.

Figure 6.- Effective gust-velocity power spectral densities for rolling moment computed for elliptic span load distribution and a range of wing-span ratios. The curves have been nondimensionalized for $\overline{w^2}$ = 0.3048 m/sec (1 ft/sec) and L* = 365.76 m (1200 ft).

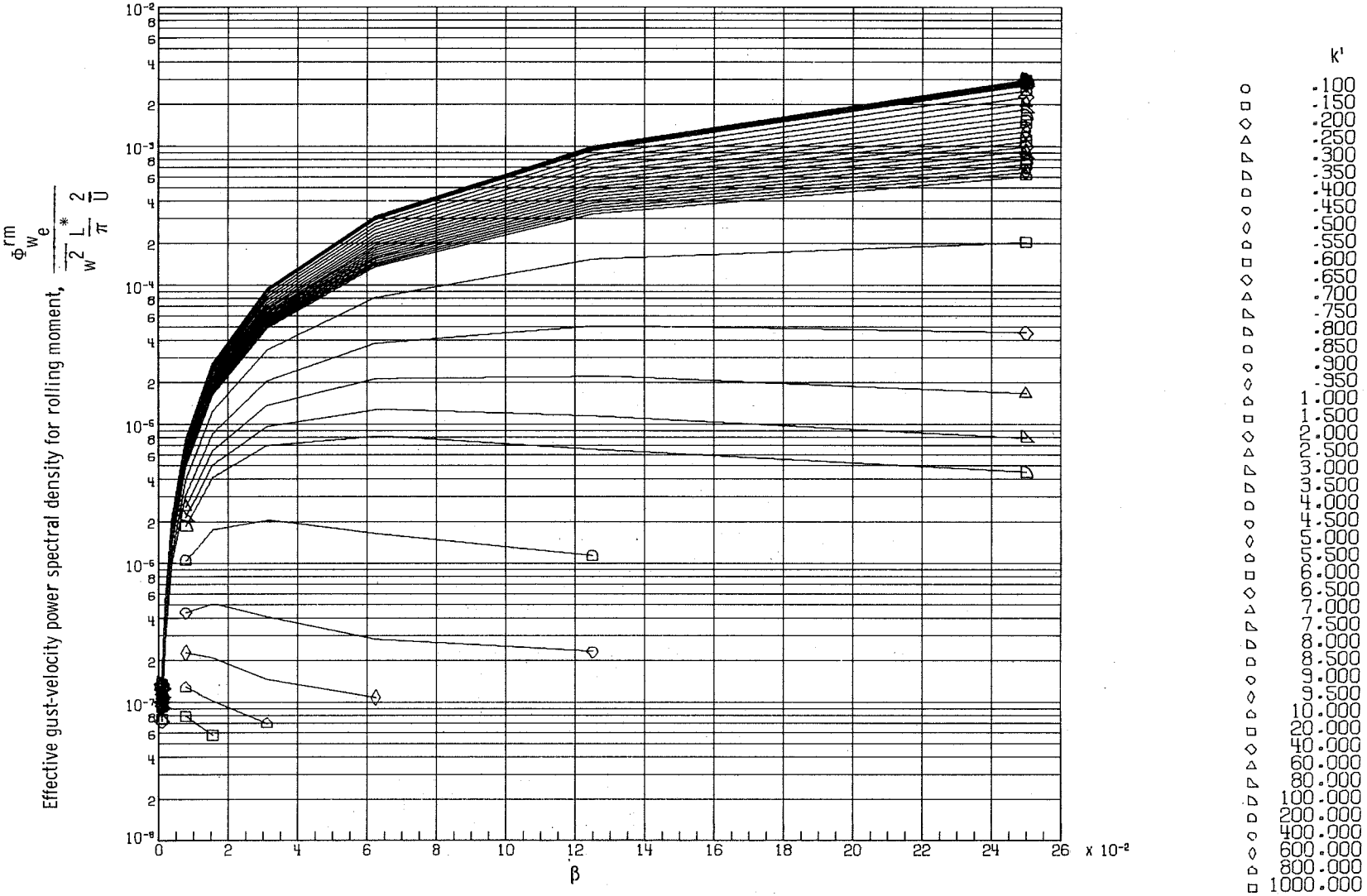

(b) Effective power spectral density plotted against wing-span ratio.

Figure 6.- Continued.

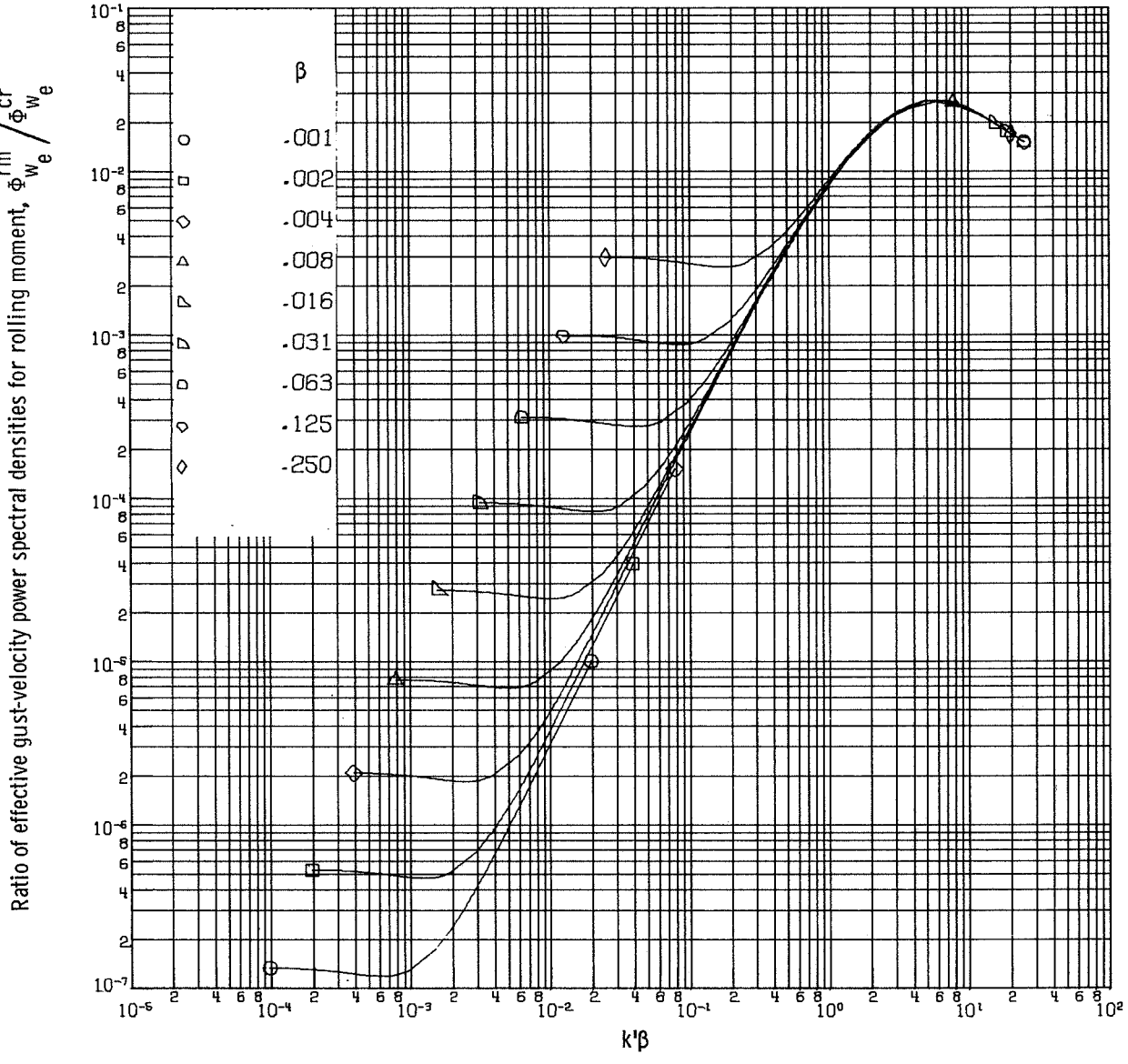

(c) Ratio of effective power spectral densities for various span ratios to that for steady rolling.

Figure 6.- Concluded.

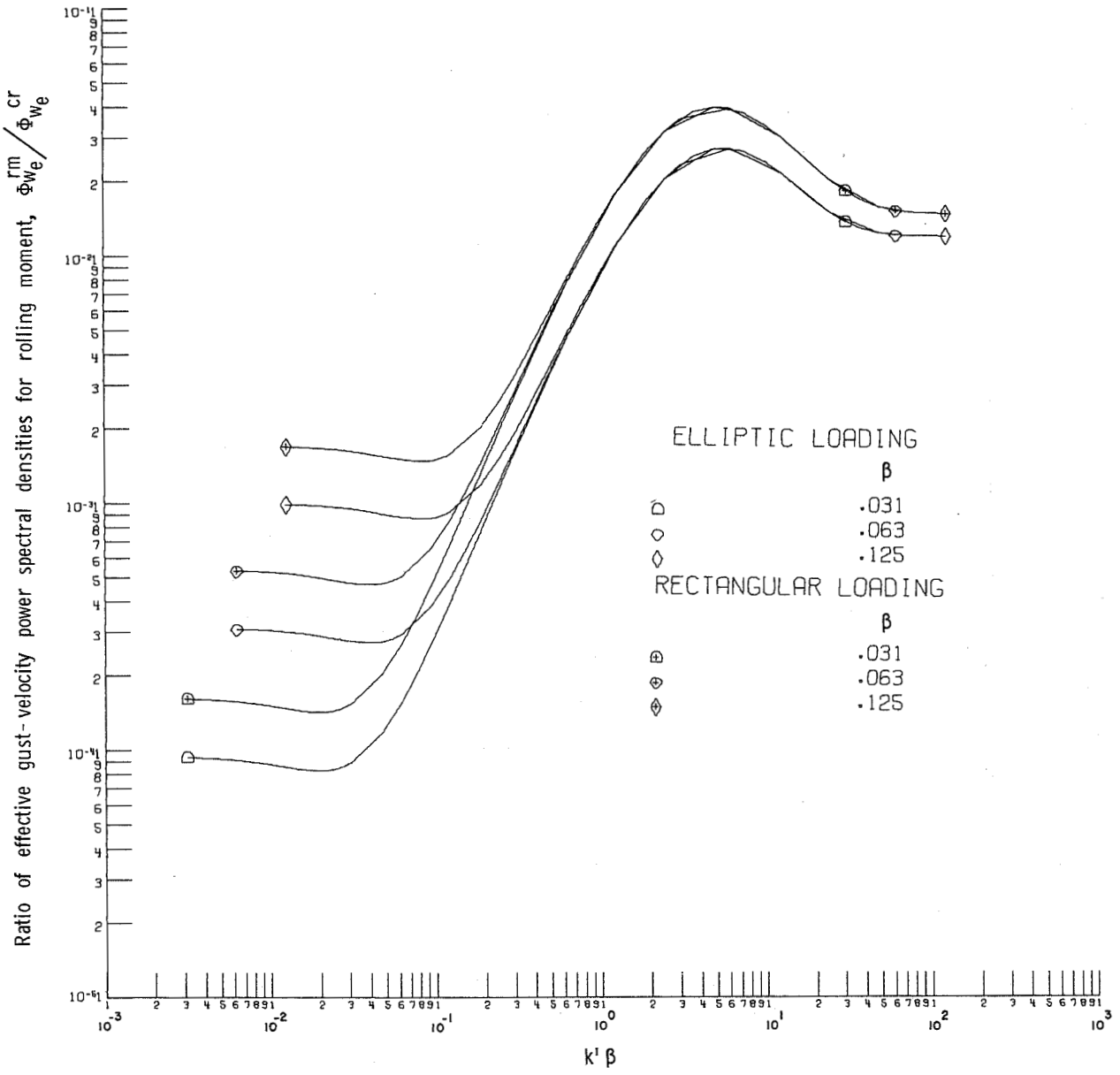

Figure 7.- Comparison of wing-span averaging effect on effective gust power spectral density for rolling moments between rectangular and elliptic span load distributions.

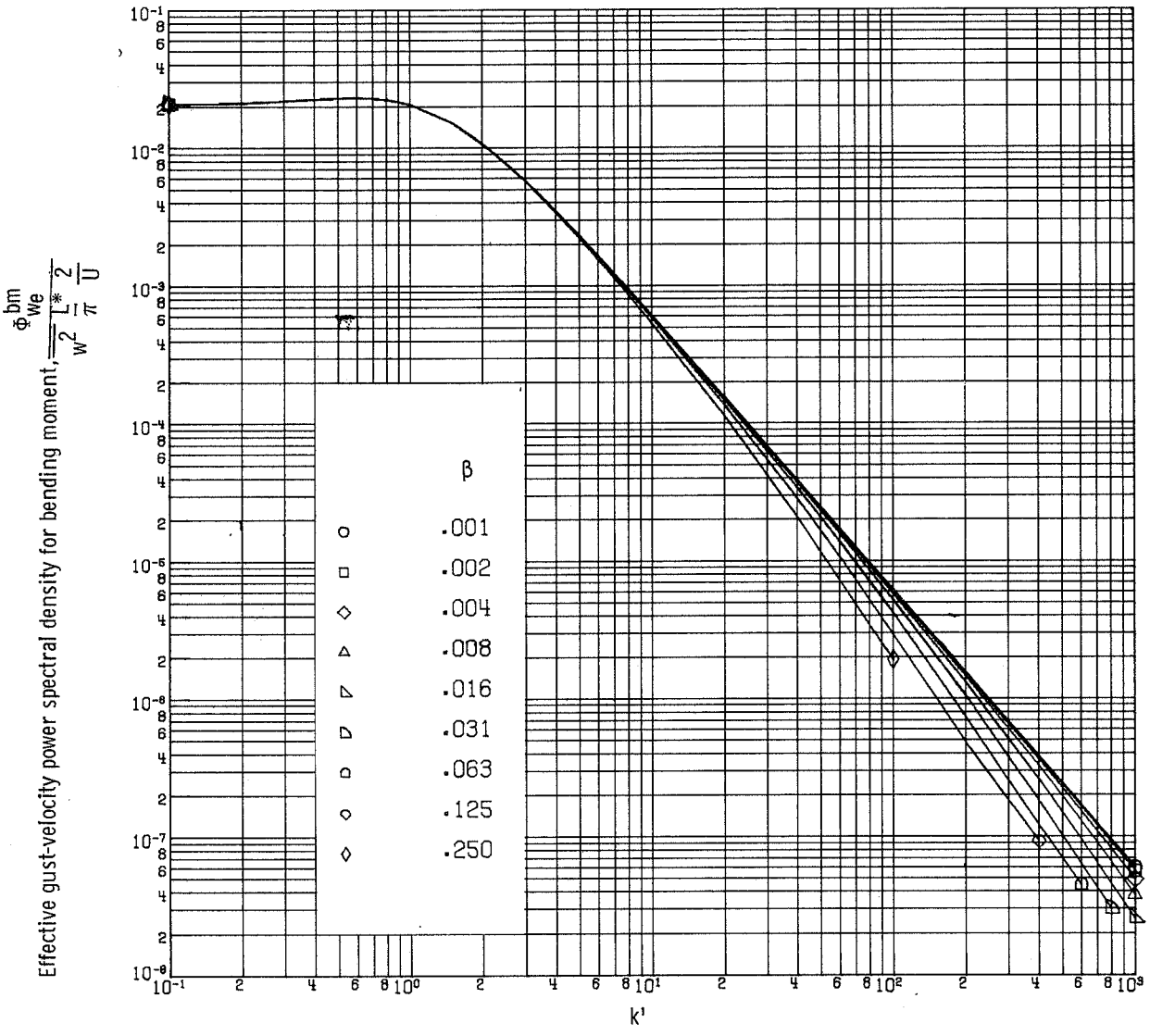

(a) Effective power spectral density plotted against nondimensional frequency for various span ratios.

Figure 8.- Effective gust-velocity power spectral densities for root chord bending moment computed for rectangular span load distribution and a range of wing-span ratios. The curves have been nondimensionalized for $\overline{w^2}$ = 0.3048 m/sec (1 ft/sec) and L* = 365.76 m (1200 ft).

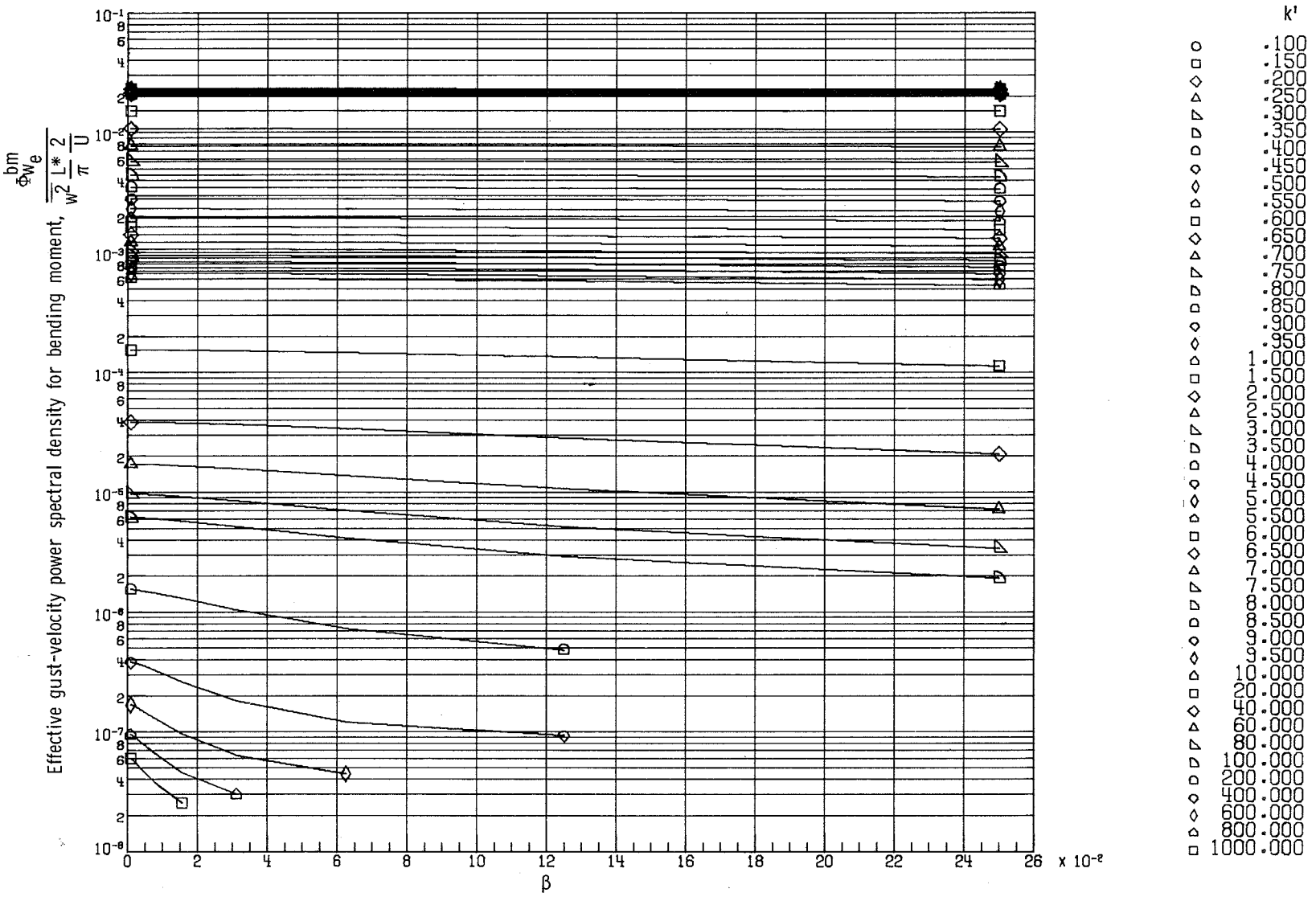

(b) Effective power spectral density plotted against wing-span ratio.

Figure 8.- Continued.

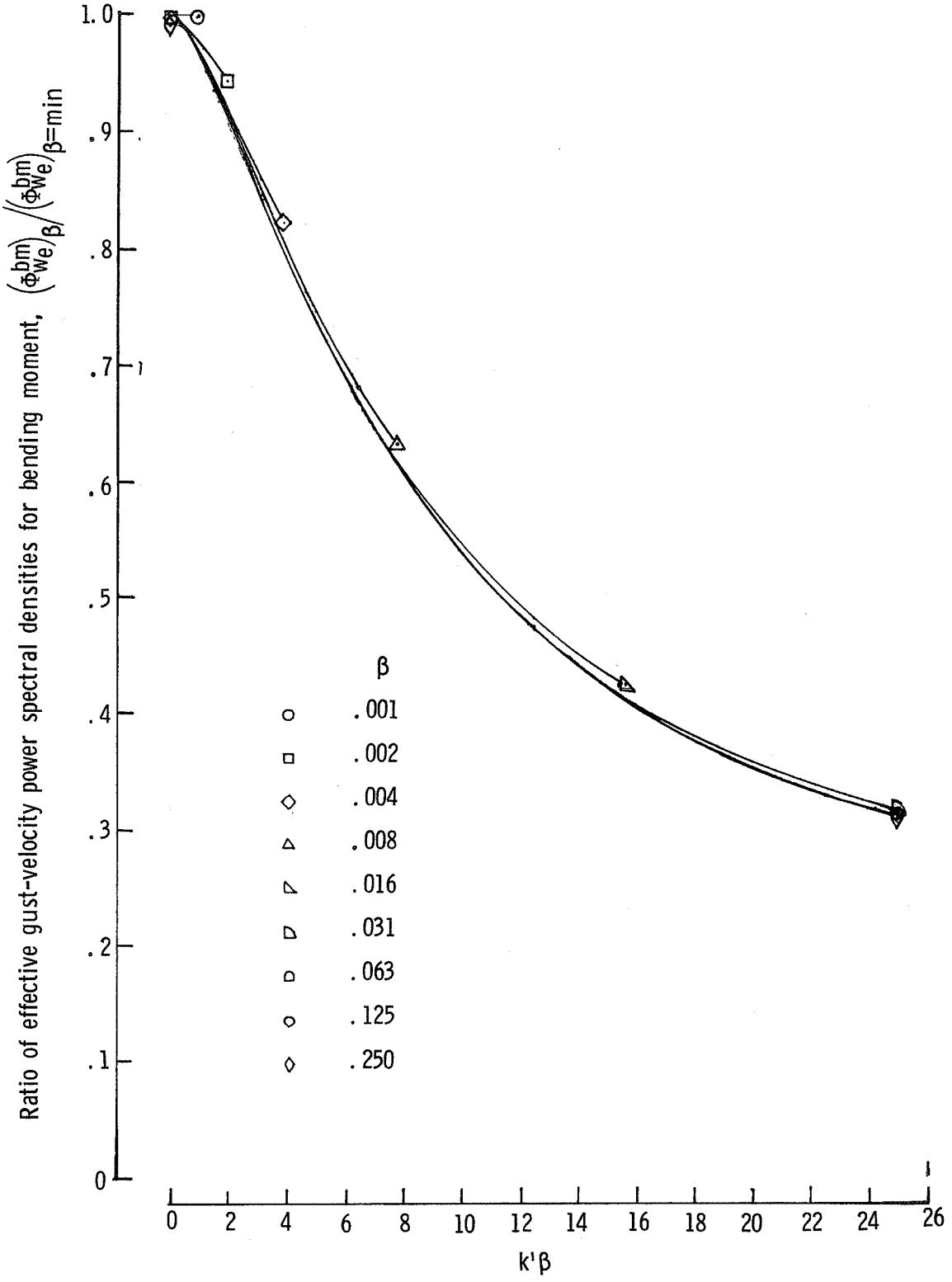

(c) Ratio of effective power spectral densities for various span ratios to that for minimum span ratio.

Figure 8.- Continued.

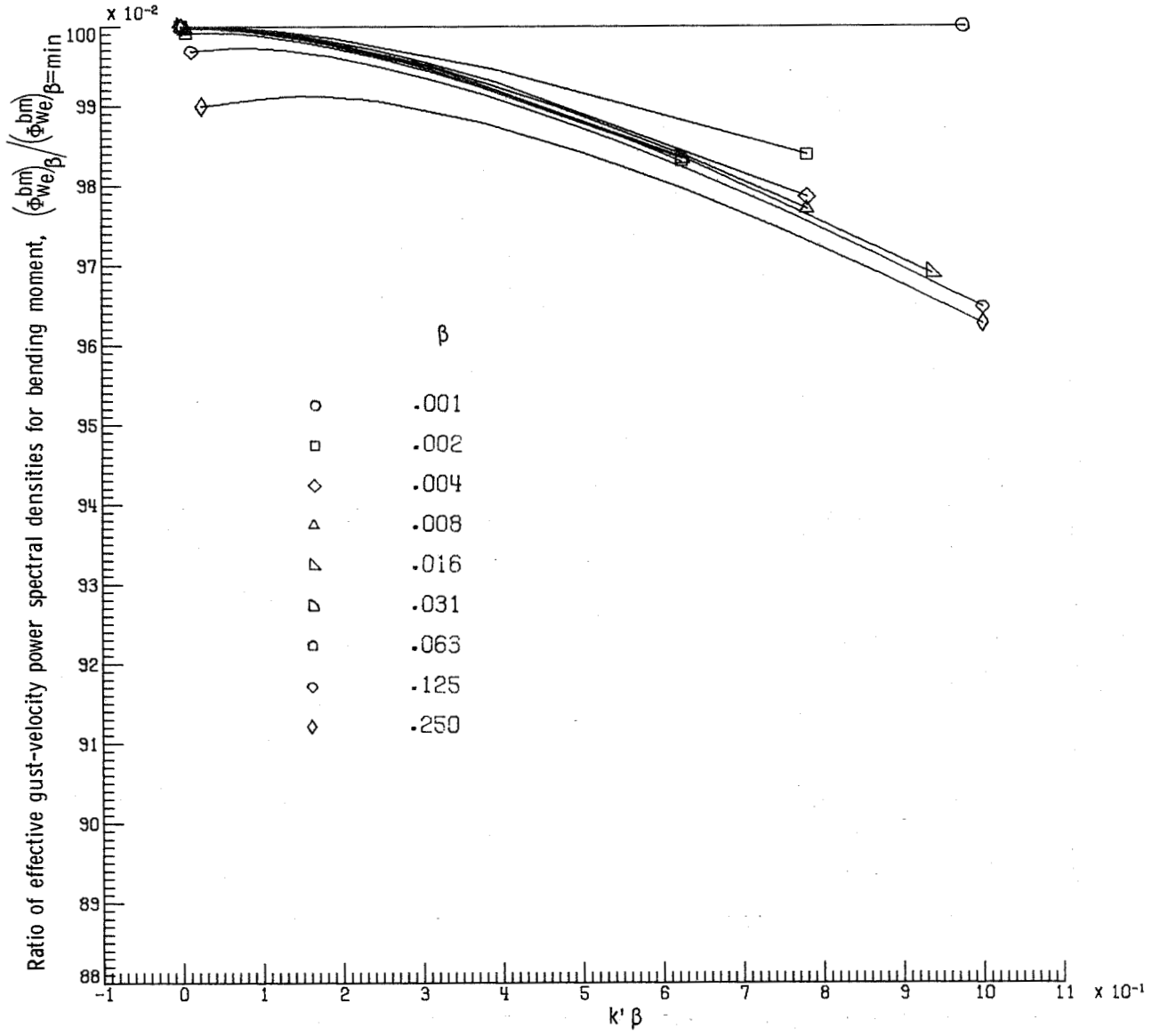

(d) Ratio of effective power spectral densities for various span ratios to that for minimum span ratios.

Figure 8.- Concluded.

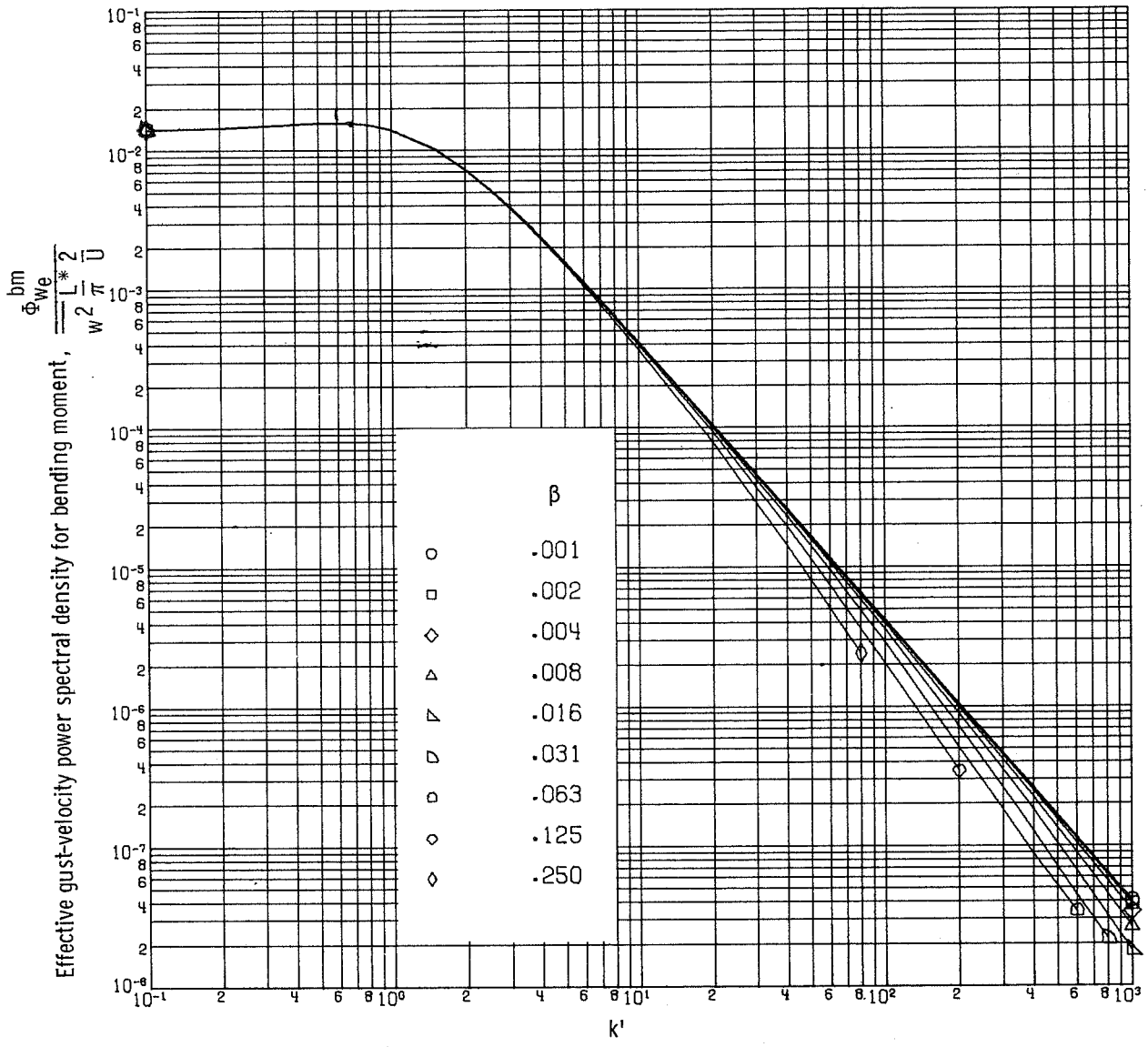

(a) Effective power spectral density plotted against nondimensional frequency for various span ratios.

Figure 9.- Effective gust-velocity power spectral densities for root chord bending moment computed for elliptic span load distribution and a range of wing-span ratios. The curves have been nondimensionalized for $\overline{w^2}$ = 0.3048 m/sec (1 ft/sec) and L* = 365.76 m (1200 ft).

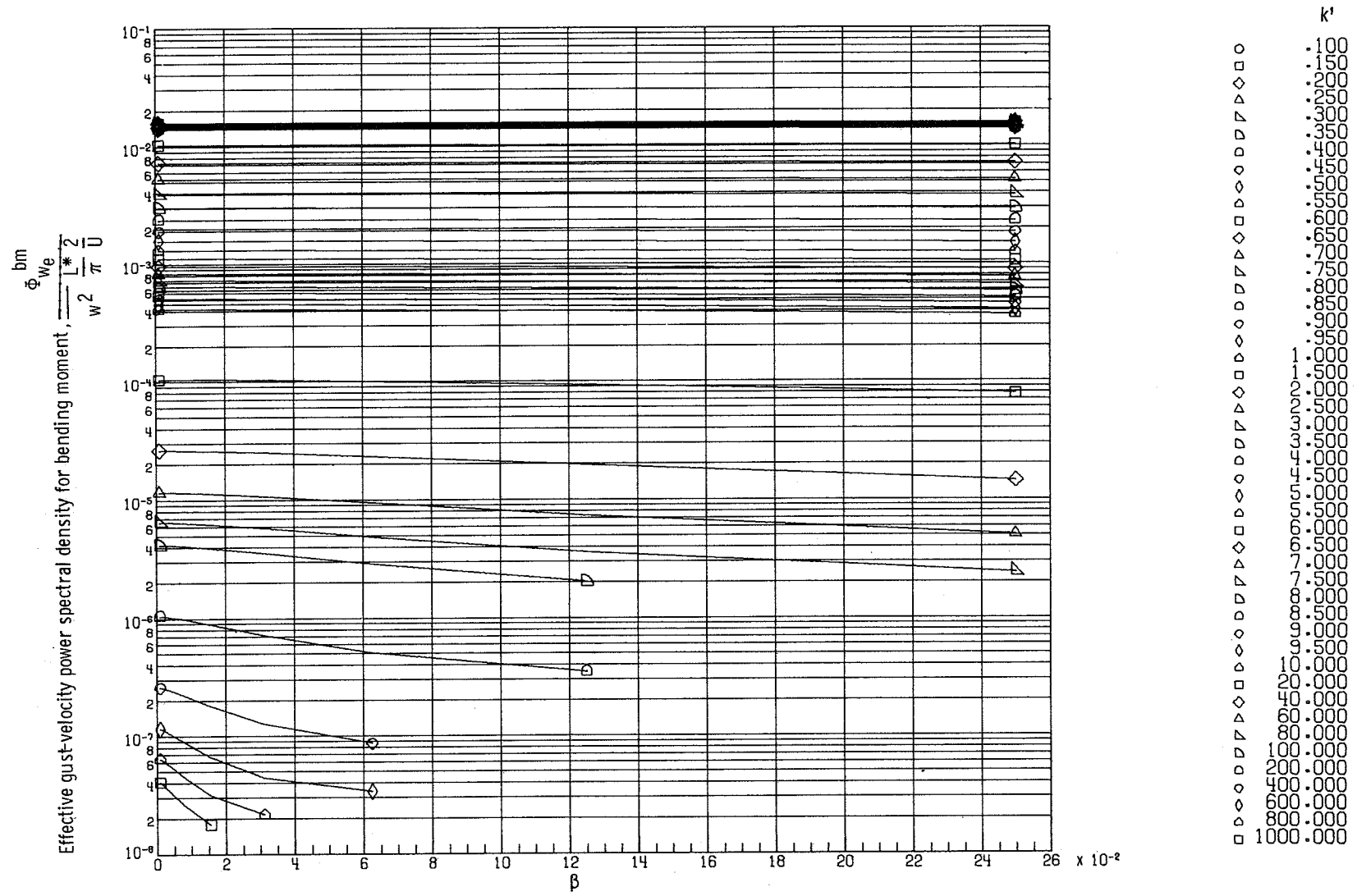

(b) Effective power spectral density plotted against wing-span ratio.

Figure 9.- Continued.

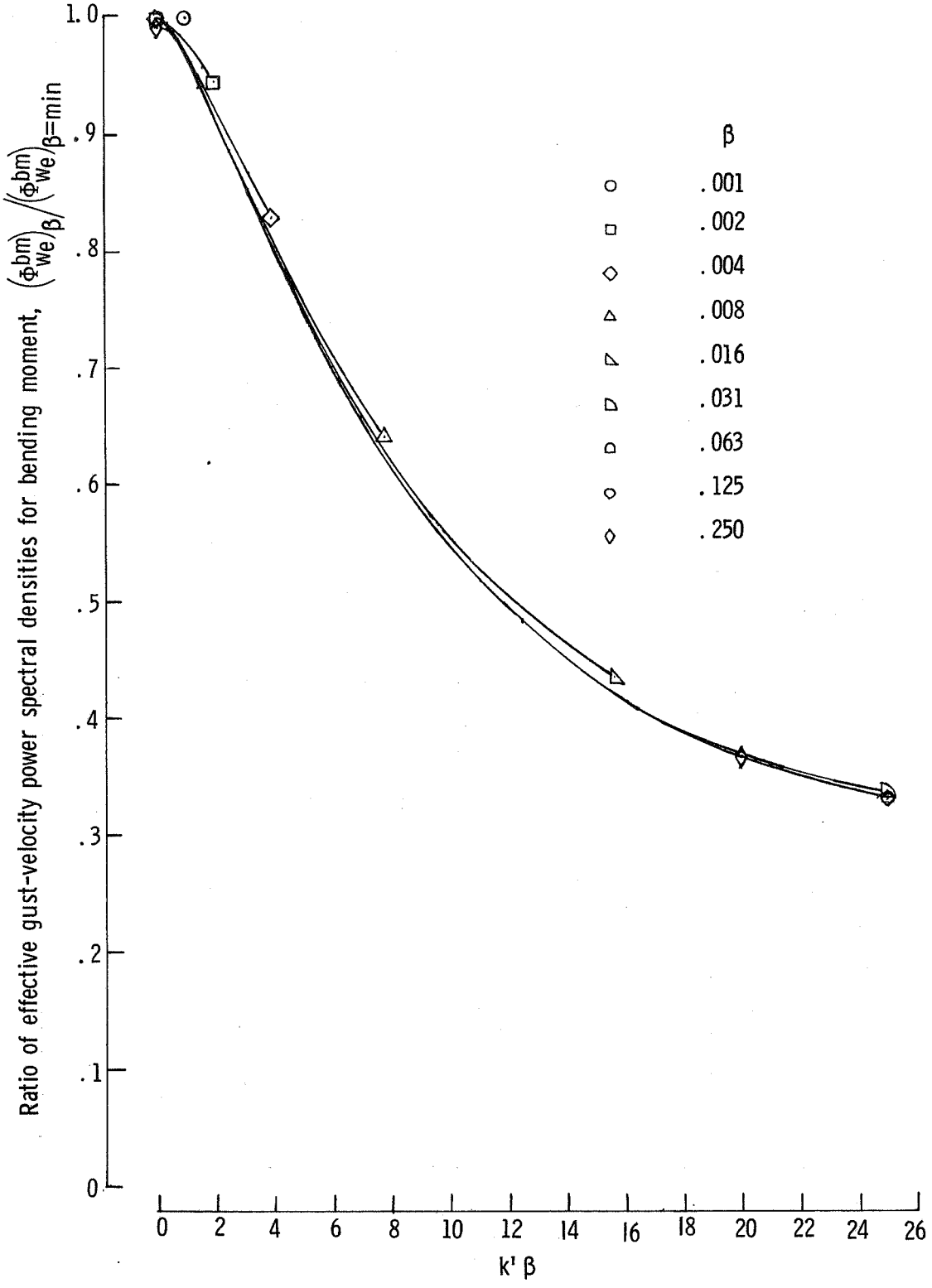

(c) Ratio of effective power spectral densities for various span ratios to that for minimum span ratio.

Figure 9.- Continued.

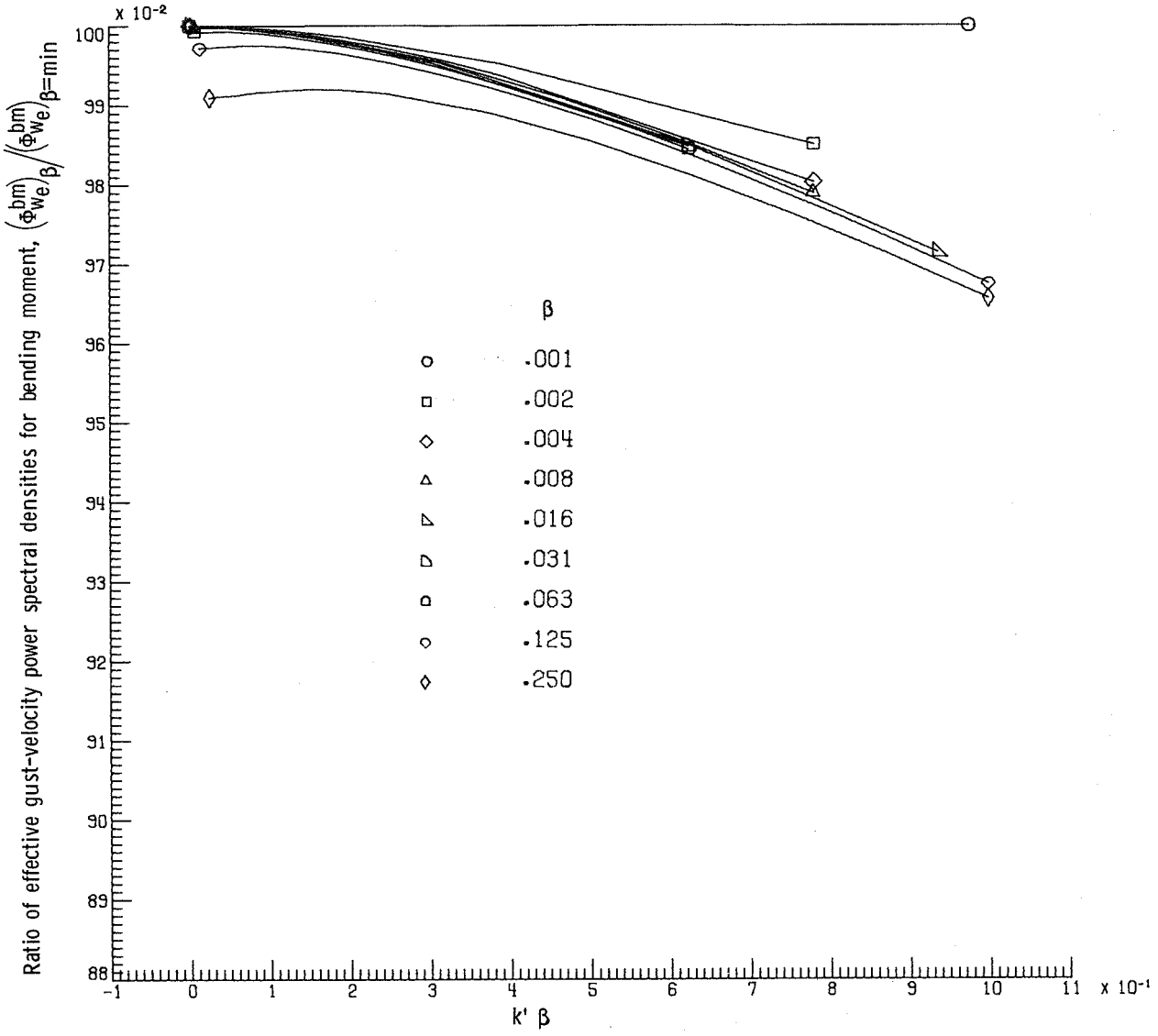

(d) Ratio of effective power spectral densities for various span ratios to that for minimum span ratio.

Figure 9.- Concluded.

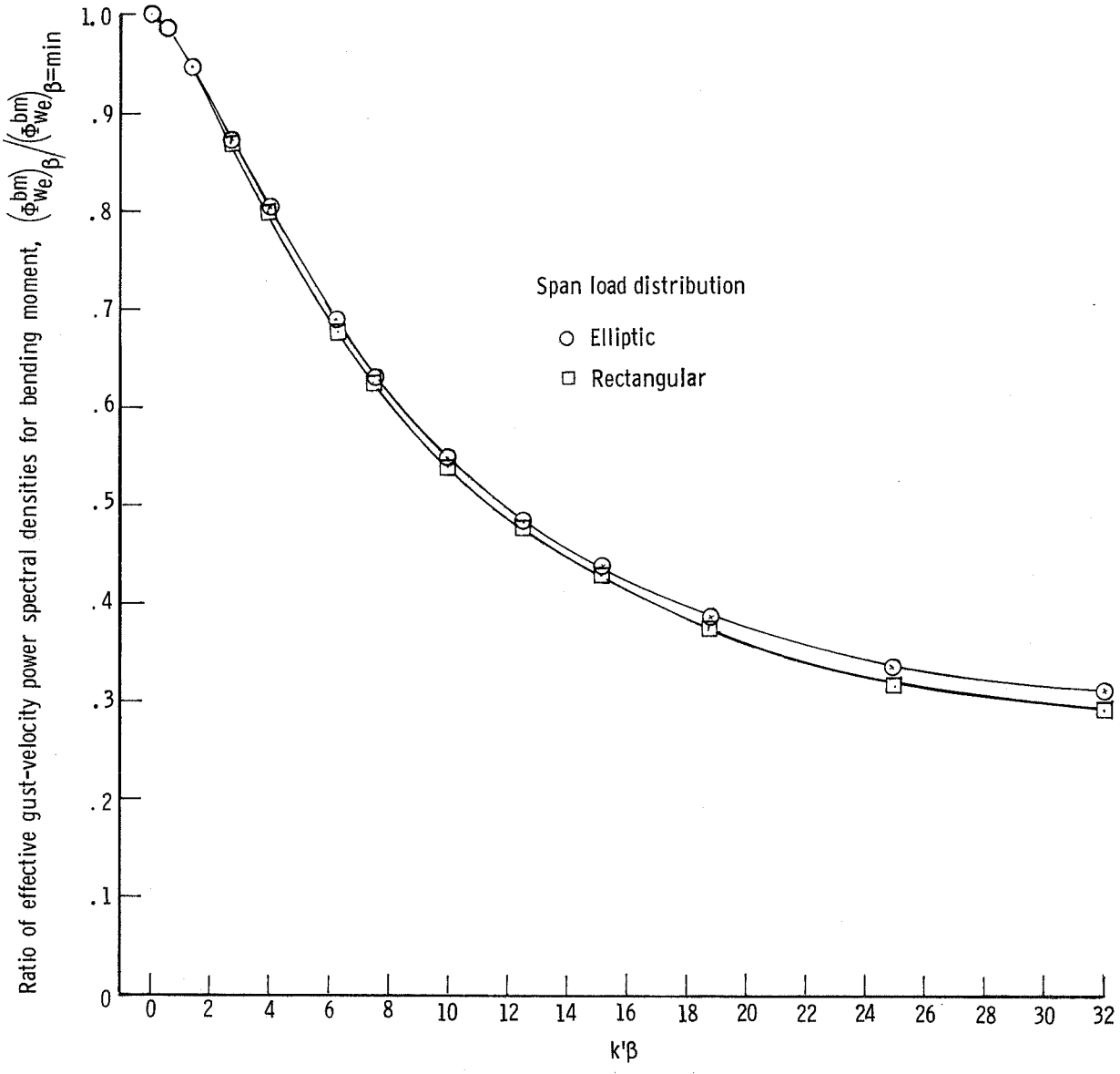

Figure 10.- Comparison of wing-span averaging effect on effective gust power spectral density for root chord bending moments between rectangular and elliptic span load distributions.

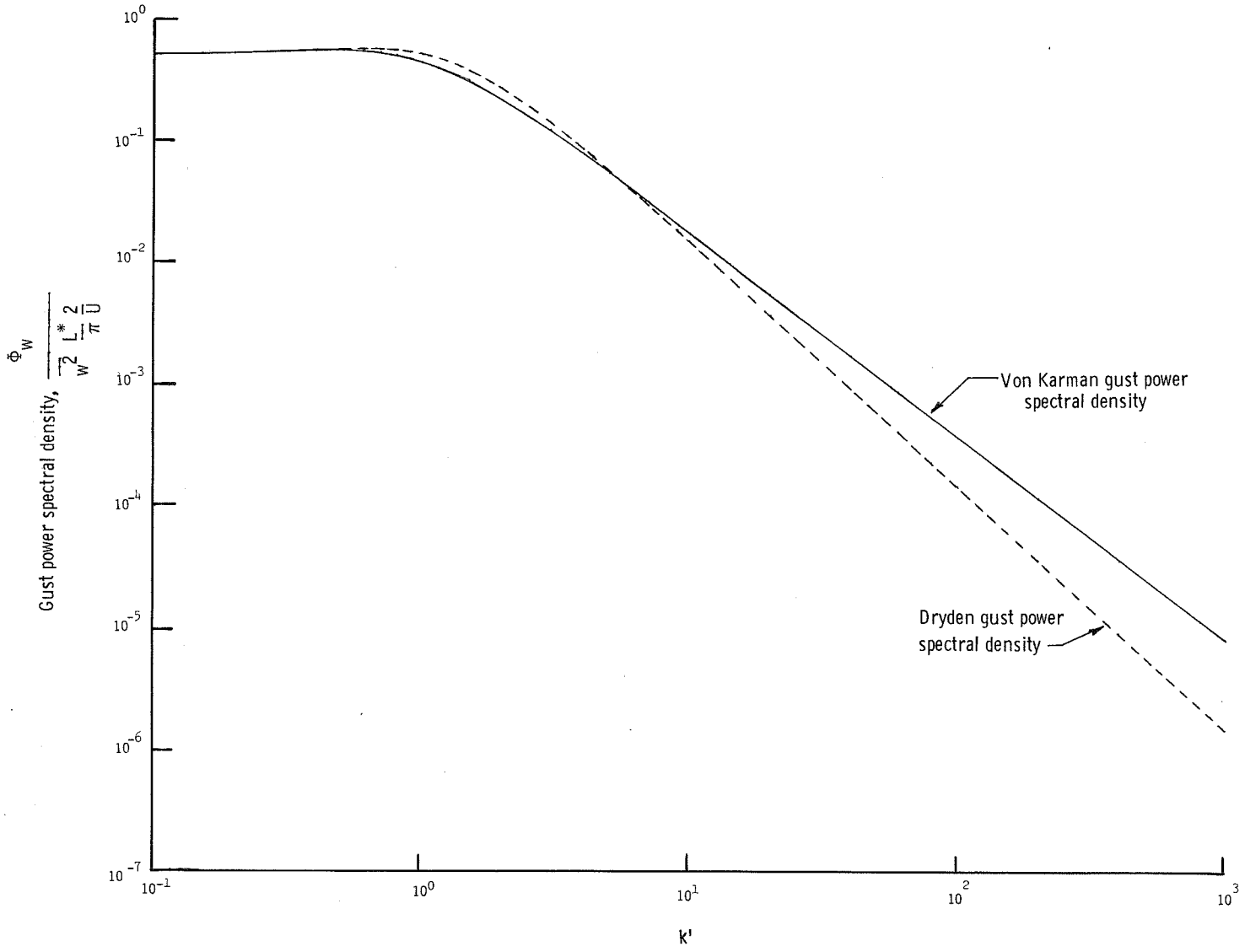

Figure 11.- Comparison of Dryden and Von Karman gust input power spectral densities.

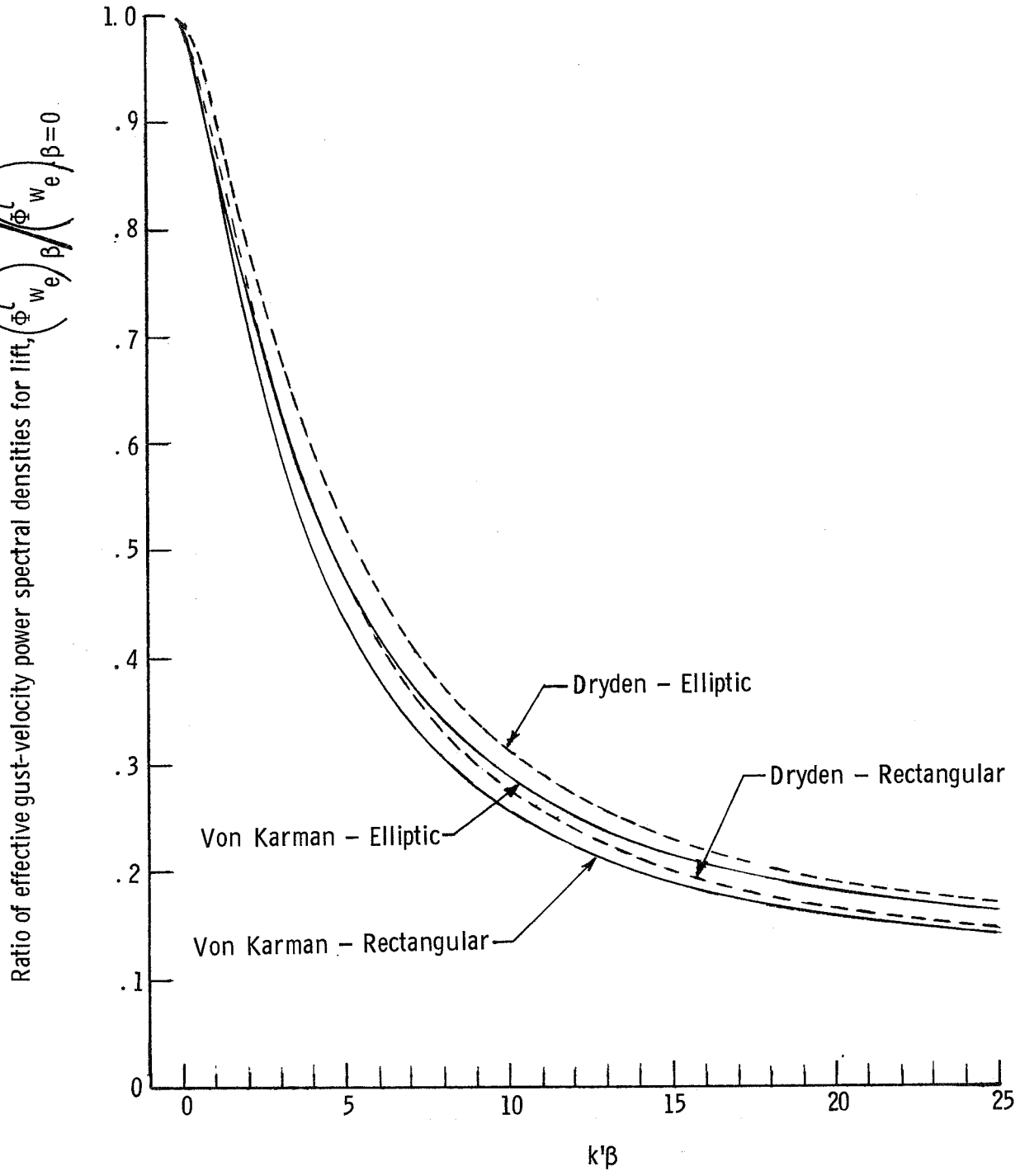

Figure 12.- Comparison of wing span averaging effect on effective gust power spectral density for lift between rectangular and elliptic span load distributions for both the Dryden and Von Karman gust input spectral representations.

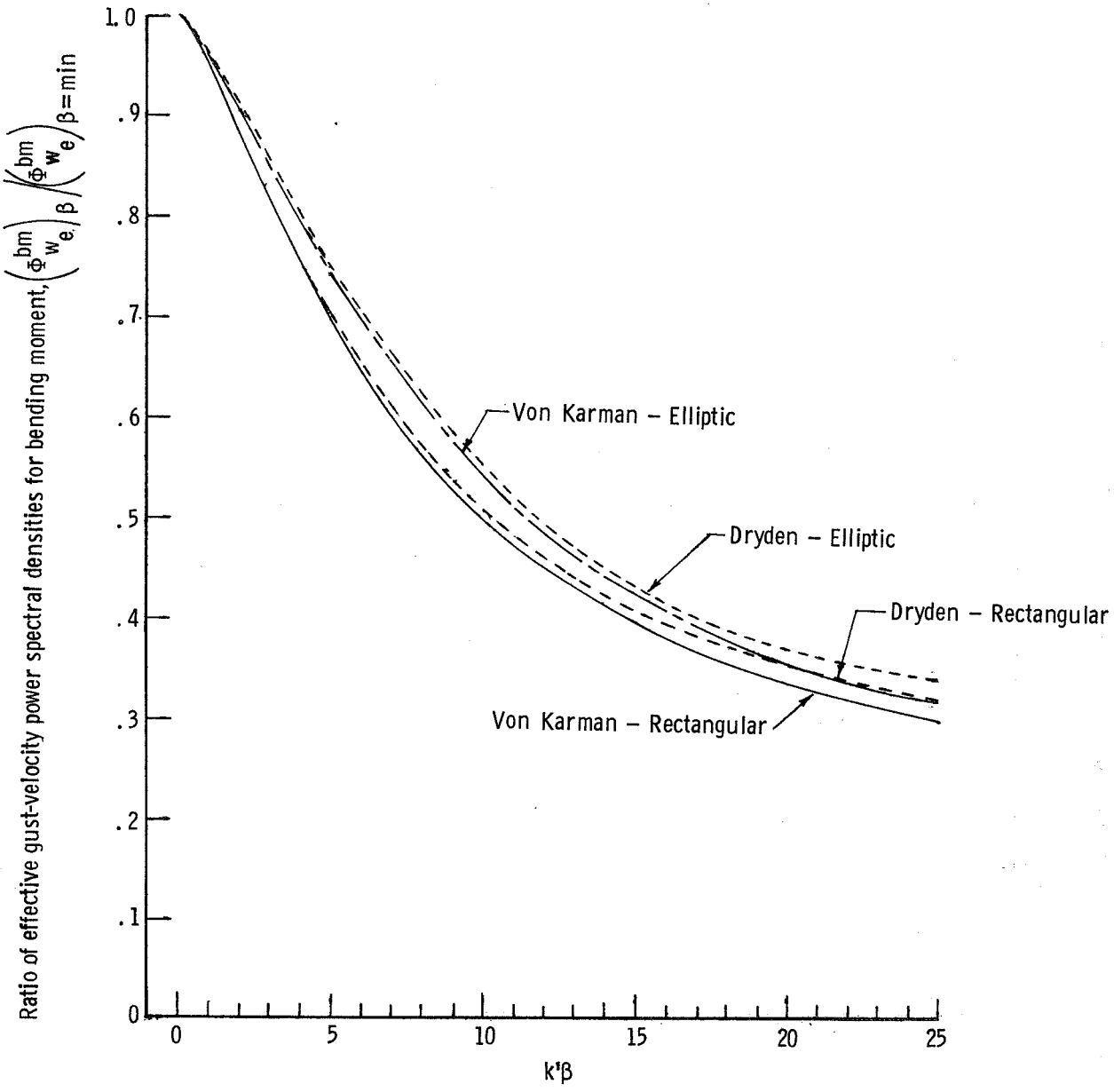

Figure 13.- Comparison of wing span averaging effect on effective gust power spectral density for root chord bending moment between rectangular and elliptic span load distributions for both the Dryden and Von Karman gust input spectral representations.

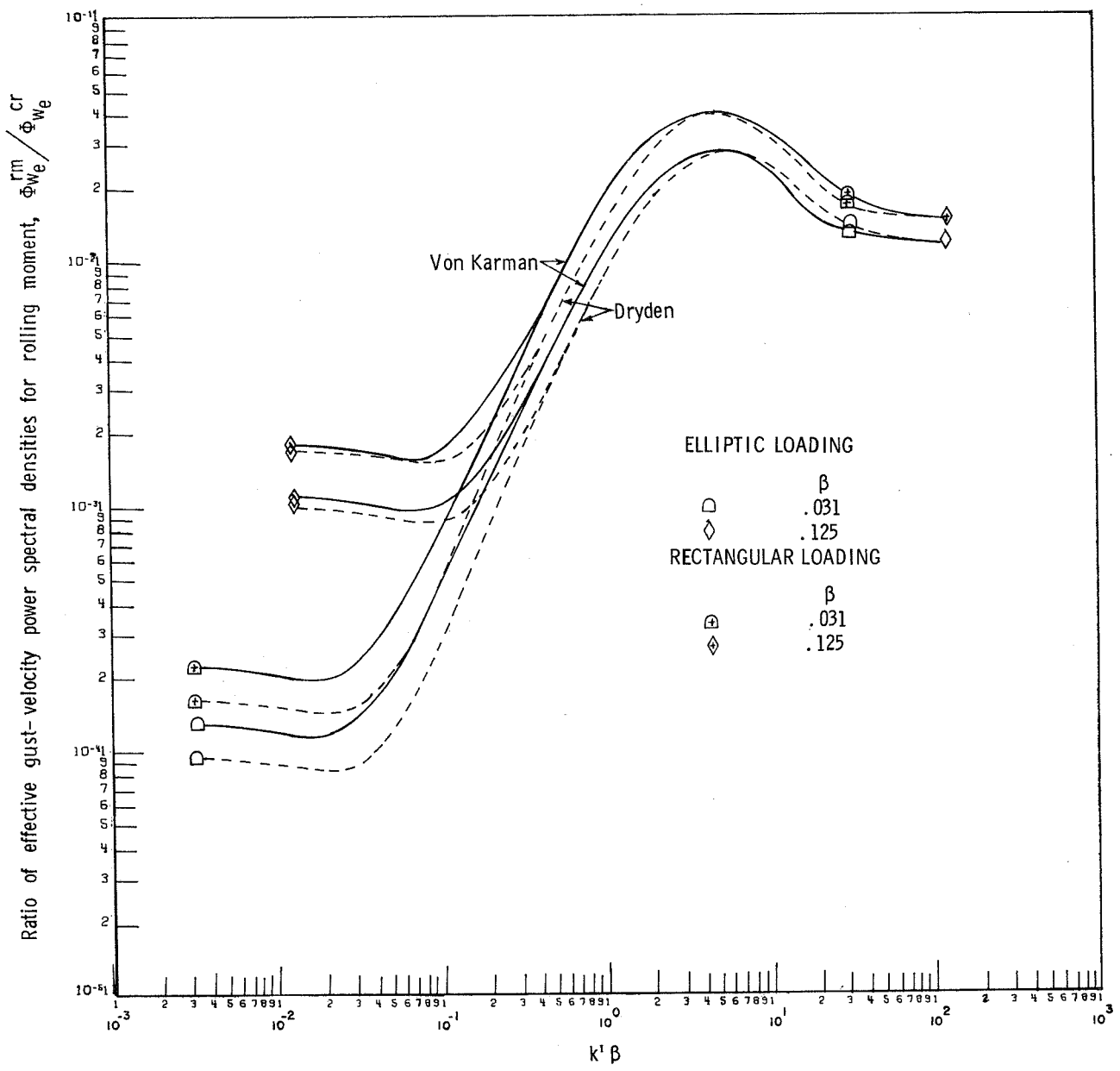

Figure 14.- Comparison of wing span averaging effect on effective gust power spectral density for rolling moment between rectangular and elliptic span load distributions for both the Dryden and Von Karman gust input spectral representations.

1. Report No.	2. Government Accession No.	3. Recipient's Catalog No.
NASA TM-78699		

4. Title and Subtitle	5. Report Date
COMPARISON OF WING-SPAN AVERAGING EFFECTS ON LIFT, ROLLING MOMENT, AND BENDING MOMENT FOR TWO SPAN LOAD DISTRIBUTIONS AND FOR TWO TURBULENCE REPRESENTATIONS	September 1978
	6. Performing Organization Code

7. Author(s)	8. Performing Organization Report No.
Jacob H. Lichtenstein	L-12014
	10. Work Unit No.
	505-10-13-03

9. Performing Organization Name and Address	11. Contract or Grant No.
NASA Langley Research Center Hampton, VA 23665	
	13. Type of Report and Period Covered
12. Sponsoring Agency Name and Address	Technical Memorandum
National Aeronautics and Space Administration Washington, DC 20546	14. Sponsoring Agency Code

15. Supplementary Notes

16. Abstract

An analytical method of computing the averaging effect of wing-span size on the loading of a wing induced by random turbulence was adapted for use on a digital electronic computer. The turbulence input was assumed to have a Dryden power spectral density. The computations were made for lift, rolling moment, and bending moment for two span load distributions, rectangular and elliptic.

Data are presented to show the wing-span averaging effect for wing-span ratios encompassing current airplane sizes. The rectangular wing-span loading showed a slightly greater averaging effect than did the elliptic loading. In the frequency range most bothersome to airplane passengers, the wing-span averaging effect can reduce the normal lift load, and thus the acceleration, by about 7 percent for a typical medium-sized transport. Some calculations were made to evaluate the effect of using a Von Karman turbulence representation. These results showed that using the Von Karman representation generally resulted in a span averaging effect about 3 percent larger.

17. Key Words (Suggested by Author(s))	18. Distribution Statement
Turbulence Unsteady lift Spanwise averaging Gusts	Unclassified - Unlimited Subject Category 02

19. Security Classif. (of this report)	20. Security Classif. (of this page)	21. No. of Pages	22. Price*
Unclassified	Unclassified	46	$4.50

* For sale by the National Technical Information Service, Springfield, Virginia 22161

NASA-Langley, 1978